

# Sunlight-driven photocatalytic mineralization of antibiotic chemical and selected enteric bacteria in water via zinc tungstate-imprinted kaolinite

Moses O. Alfred, Chidinma G. Olorunnisola, Temidayo T. Oyetunde, Peter Dare, Raquel R. C. Vilela, Andrea de Camargo, Nurudeen A. Oladoja, Martins O. Omorogie, Olumide D. Olukanni, Artur de Jesus Motheo & Emmanuel I. Unuabonah

To cite this article: Moses O. Alfred, Chidinma G. Olorunnisola, Temidayo T. Oyetunde, Peter Dare, Raquel R. C. Vilela, Andrea de Camargo, Nurudeen A. Oladoja, Martins O. Omorogie, Olumide D. Olukanni, Artur de Jesus Motheo & Emmanuel I. Unuabonah (2022) Sunlight-driven photocatalytic mineralization of antibiotic chemical and selected enteric bacteria in water via zinc tungstate-imprinted kaolinite, Green Chemistry Letters and Reviews, 15:3, 705-723, DOI: [10.1080/17518253.2022.2124889](https://doi.org/10.1080/17518253.2022.2124889)

To link to this article: <https://doi.org/10.1080/17518253.2022.2124889>



© 2022 The Author(s). Published by Informa UK Limited, trading as Taylor & Francis Group



View supplementary material [↗](#)



Published online: 10 Oct 2022.



Submit your article to this journal [↗](#)



Article views: 165



View related articles [↗](#)



View Crossmark data [↗](#)

RESEARCH ARTICLE



## Sunlight-driven photocatalytic mineralization of antibiotic chemical and selected enteric bacteria in water via zinc tungstate-imprinted kaolinite

Moses O. Alfred<sup>a,b,c</sup>, Chidinma G. Olorunnisola<sup>a</sup>, Temidayo T. Oyetunde<sup>b</sup>, Peter Dare<sup>a</sup>, Raquel R. C. Vilela<sup>d</sup>, Andrea de Camargo<sup>d</sup>, Nurudeen A. Oladoja<sup>e</sup>, Martins O. Omorogie<sup>ib,a,b</sup>, Olumide D. Olukanni<sup>a,f</sup>, Artur de Jesus Motheo<sup>c</sup> and Emmanuel I. Unuabonah<sup>ib,a,b</sup>

<sup>a</sup>African Centre of Excellence for Water and Environment Research (ACEWATER), Redeemer's University, Ede, Nigeria; <sup>b</sup>Department of Chemical Sciences, Redeemer's University, Ede, Nigeria; <sup>c</sup>São Carlos Institute of Chemistry, University of São Paulo, São Carlos, Brazil; <sup>d</sup>São Carlos Institute of Physics, University of São Paulo, São Carlos, Brazil; <sup>e</sup>Hydrochemistry Research Laboratory, Department of Chemical Sciences, Adekunle Ajasin University, Akungba-Akoko, Nigeria; <sup>f</sup>Department of Biochemistry, Redeemer's University, Ede, Nigeria

### ABSTRACT

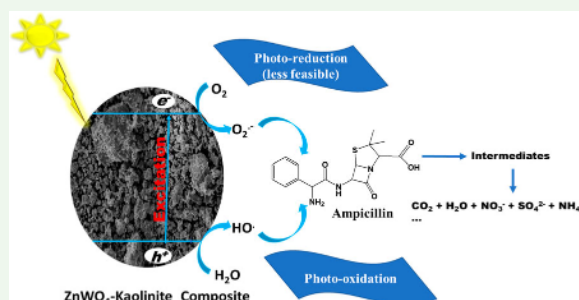
This study reports the synthesis of sunlight-active zinc oxide-tungstate-kaolinite photocatalytic composite prepared via a green process (solvent-free mechano-thermal process) at an optimum temperature of 500°C for 1 h in a furnace. Electron Paramagnetic Resonance (EPR) study suggests the presence of  $W^{5+}$  defect states in the prepared photocatalytic composite (ZnWK-5), which is responsible for its photoactivity in visible light. Results from further analysis show that hole ( $h^+$ ) and superoxide radical ( $O_2^-$ ) are the major contributors to the photocatalytic efficiency of ZnWK-5 photocatalytic composite. This photocatalytic composite was used to treat water containing an antibiotic chemical-ampicillin (AMP) under sunlight. Mass spectrometry analysis of the treated water suggests that the mechanism of photodegradation of AMP is via several bond and ring cleavages, including amide bond, phenyl ring, and  $\beta$ -lactam ring cleavages. These cleavage reactions were followed by subsequent mineralization of ca. 98% after 5 h without the formation of toxic products. The introduction of phosphate and carbonate anions had a serious negative impact on the photocatalytic activity of the composite. However, the photocatalytic composite completely disinfected water contaminated with gram-(–ve) and gram-(+ve) bacteria. Even after five re-use cycles, the photocatalytic composite maintained a 90% photodegradation efficiency of ampicillin in water.

### ARTICLE HISTORY

Received 3 May 2022  
Accepted 9 September 2022

### KEYWORDS




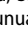
Kaolinite; photo-mineralization; ampicillin; water disinfection; Advanced Oxidation Processes (AOP)




## 1. Introduction

There have been several reports on disease outbreaks around the world and especially in developing countries (1). Most of these outbreaks are related to poor quality of drinking water and food. In fact, roughly 88% of diarrhea diseases reported are linked to poor quality of water

supply and poor hygiene (1). In most cases, these outbreaks lead to several deaths in developing countries. It has been reported recently that > 1.3 million deaths of children are caused by diarrheal illness worldwide every year (2). Diarrheal as well as some other water-borne diseases are caused by pathogenic organisms. In

**CONTACT** Moses O. Alfred  [alfredm@run.edu.ng](mailto:alfredm@run.edu.ng)  African Centre of Excellence for Water and Environment Research (ACEWATER), Redeemer's University, PMB 230, Ede, Osun State, Nigeria; Department of Chemical Sciences, Redeemer's University, PMB 230, Ede, Osun State, Nigeria; São Carlos Institute of Chemistry, University of São Paulo, Av. Trabalhador São-carlense 400, 13566-590, São Carlos, Brazil; Emmanuel I. Unuabonah  [unuabonahe@run.edu.ng](mailto:unuabonahe@run.edu.ng)  African Centre of Excellence for Water and Environment Research (ACEWATER), Redeemer's University, PMB 230, Ede, Osun State, Nigeria; Department of Chemical Sciences, Redeemer's University, PMB 230, Ede, Osun State, Nigeria

 Supplemental data for this article can be accessed online at <https://doi.org/10.1080/17518253.2022.2124889>.

© 2022 The Author(s). Published by Informa UK Limited, trading as Taylor & Francis Group

This is an Open Access article distributed under the terms of the Creative Commons Attribution License (<http://creativecommons.org/licenses/by/4.0/>), which permits unrestricted use, distribution, and reproduction in any medium, provided the original work is properly cited.

order to treat diseases associated with pathogens, several pharmaceutical chemicals were developed. However, even though these pharmaceutical chemicals are known to be quite effective against these pathogens, they are now identified as a new class of contaminants of emerging concern when found in water (3). They are introduced into the aquatic environment as by-products from human waste and from anthropogenic activities. Of much concern currently, is that some of these pharmaceutical chemicals are only effective for a limited time when used to treat pathogenic diseases in humans. The pathogens soon develop resistance to them (3, 4).

Drug resistance is one of the major challenges facing the success of several drugs today, reducing the therapeutic potential of these drugs (5). This could lead to more serious disease outbreaks (6, 7). This resistance to pharmaceutical chemicals shown by microbial agents is partly due to the pseudo-persistent nature of these chemicals in water. Worse still, most water and wastewater treatment plants are not even suitably designed to handle the total remediation of these pharmaceutical chemicals from water (8, 9).

However, treatment processes such as adsorption (10), membrane filtration (11–13), nanofiltration and reverse osmosis (14), electro-coagulation (15), adsorption and oxidation (16), advanced oxidation process (17), and heterogeneous photocatalysis (18–20) have been proposed as possible remediation techniques for pharmaceutical chemical contaminants (PCCs) in water and wastewater. Yet, some of these processes only transform the pollutants into chemical compounds that could make the treated wastewater potentially more hazardous than its untreated form (21). For instance, biological treatment processes are known to create an enabling environment for the development and spread of antibiotic resistance genes (5). This is because, during this process, bacteria are continuously mixed with antibiotics at sub-inhibitory concentrations in the treatment plants leading to antibiotic resistance development in the bacteria. This makes the treatment plant serve as a major reservoir of antibiotics and ARGs (5).

The heterogeneous photocatalytic process is not left out. The problem of degradation of pharmaceutical chemicals to more harmful by-products persist, such that the treated water is potentially 'poisoned' before they are consumed by humans. Another potential challenge with the use of heterogeneous photocatalytic process for the removal of pharmaceutical chemicals from water is the fast recombination of electron-hole pair and the low quantum yield of some photocatalysts, reducing their efficiency in treating water. Worse still, is the high cost of photocatalyst production, poor recovery of photocatalysts after application, and the expensive

requirement for running UV lamps (for UV-active photocatalysts) especially in developing countries like in Africa faced with huge power supply deficit. Hence, research is now focused on developing materials that can effectively and efficiently remove PCCs from water, especially in drinking water, via a green process called mineralization (converting pharmaceutical chemical moieties to  $\text{CO}_2$ ,  $\text{H}_2\text{O}$  and other smaller non-harmful molecules or ions).

This study reports the successful development of a  $\text{ZnWO}_4\text{-ZnO/kaolinite}$  photocatalytic composite material for mineralization of ampicillin and bacteria in water. The use of kaolinite in this photocatalytic composite is justified on the basis of its potential to enhance charge separation through the formation of a type II staggered band heterostructure and promote the production of reactive radicals via an oxygen-rich microenvironment (22). This type II staggered band heterostructure have been shown to improve catalysts dispersion, ameliorate catalysts agglomeration and enhance the effective recovery of bare catalysts for reuse (23, 24). Although  $\text{ZnWO}_4$  is relatively cheap, possesses high photosensitivity, excellent chemical stability, and is non-toxic, it is however, only very efficient in the UV region of the electromagnetic spectrum and much less in the visible light region. This is mainly due to its large bandgap of ca. 3.5 eV (25, 26). To enhance the photo-response of  $\text{ZnWO}_4$  in the solar region (which is free and contain visible light portion), carbon-doping was employed. It is known that carbon doping can suppress charge recombination through intra-composite electron transfer (27, 28). A carbon-rich organic-inorganic precursor (zinc acetate) was selected and used for *in situ* carbon-doping of the prepared composite.

For the sake of this study, ampicillin (AMP) was selected as model pharmaceutical contaminant. This is premised on several reports confirming their presence in water (29, 30) and being a conventional drug used globally. Furthermore, it is a broad-spectrum antibiotic used globally to treat against gram-positive and gram-negative bacterial infections. Four bacteria: gram-negative (*Escherichia coli*, *Salmonella typhi*) and gram-positive (*Bacillus cereus*, *Staphylococcus aureus*) were used to study the disinfecting property of selected photocatalytic composite material. These bacteria were chosen because they are commonly reported in African water especially in the resistant form (31).

## 2. Materials and methods

Ampicillin (Sigma-Aldrich), sodium tungstate (97%), zinc acetate (Sigma-Aldrich, 97%), ampicillin (Sigma-Aldrich, 99%), methanol (Honeywell, HPLC grade), and

phosphoric acid (Sigma-Aldrich, 99%) were used as received. Raw kaolinite clay was sourced from Redemption City, Mowe (6° 48' 0" N, 3° 26' 0" E.), Ogun State, Nigeria. The kaolinite clay was purified and processed for use by the method provided in Adebowale et al. (32).

### 2.1. Preparation of the photocatalytic composite

The composites were prepared using a green solventless mechanochemical method of synthesis. This was achieved via the grinding of kaolinite,  $\text{Na}_2\text{WO}_4 \cdot 2\text{H}_2\text{O}$  and  $\text{Zn}(\text{CH}_3\text{CO}_2)_2$  to obtain a homogenous paste. This paste was allowed to age in an oven for 12 h at 100°C. This was followed by thermal treatment in air using a furnace held at 300°, 500°C or 700°C at a heating rate of 10°C/min and held for 1 h at the specified temperature to obtain ZnWK-3, ZnWK-5, and ZnWK-7 composites respectively. To understand the impact of the components of the composites on the physico-chemical and optical properties of the photocatalyst, analogs were prepared (i) without  $\text{Na}_2\text{WO}_4$  to obtain ZnK composite material and (ii) without  $\text{Zn}(\text{CH}_3\text{CO}_2)_2$  to obtain WK composite material at a calcination temperature of 500°C. The choice of this temperature for calcination is based on a preliminary result (not provided in this study) that suggests that the most efficient photocatalytic material can be obtained at this temperature. The resulting composites were washed thoroughly with deionized water, dried at 100°C in a laboratory oven, and stored in glass containers for further use.

### 2.2. Characterization of photocatalyst composites

The crystallinity and mineral composition of the prepared materials were determined via X-ray diffraction (XRD) using a Bruker D8 Advance X-ray diffractometer. The surface morphology and elemental composition were determined by scanning electron microscopy (ZEISS LEO 440 Scanning Electron Microscope) operated at 5 kV accelerating voltage. Fourier transformed infrared spectroscopy (FTIR) spectra for the composites were obtained from Shimadzu FT-IR 8400S (class 1, Laser product) spectrophotometer. Lambda 1050 PerkinElmer UV/Vis/NIR spectrophotometer was used to obtain the absorption spectra of the prepared composites and their corresponding apparent band gaps were estimated using the Tauc equation (33).

$$\alpha h\nu = A(h\nu - E_g)^{\frac{1}{2}} \quad (1)$$

Photoluminescence spectroscopy was carried out using a Horiba iHR320 Photoluminescence Microspectrometer at

excitation wavelength of 380 nm (based on the absorption maximum obtained from UV/Vis analysis). All measurements were performed at room temperature. Continuous-Wave Electron Paramagnetic Resonance (CW-EPR) analysis was performed on the most efficient composite at room temperature in a Bruker ELEXSYS E580 spectrometer operating at X-Band (~9.5 GHz) with a modulation amplitude of 0.5 G and power level of 64 mW.

### 2.3. Photodegradation of contaminants

An initial kinetic study to determine the efficiencies of the composites was carried out by contacting 100 mL of 50 mg/L solutions of AMP (Figure 1) with 100 mg/L of the composites. The mixture were agitated for 120 min under solar irradiation on bright days (usually between 10:00 h and 17:00 h). The solar spectrum during this period of the day is as presented in our previous study (8). Aliquots (1 mL) were collected after 120 min reaction time, filtered with 0.45 µm PTFE syringe filters and analyzed for residual AMP concentration. The residual AMP concentration was quantified using Shimadzu HPLC equipment with a degassing chamber DGU-20, quaternary pump (LC10AD), a Column oven (CTO10AS) and a UV/VIS detector (SPD10AD). Elution was achieved with a mixture of 40% methanol and 60%, milli-Q water (0.1%  $\text{H}_3\text{PO}_4$ ) at a flow rate of 0.4 mL/min, using an injection volume of 20 µL. Separation was achieved with a Agilent Zorbax SB-C18 (5 µm, 4 × 250 mm) reverse phase column. The degree of degradation was calculated as:

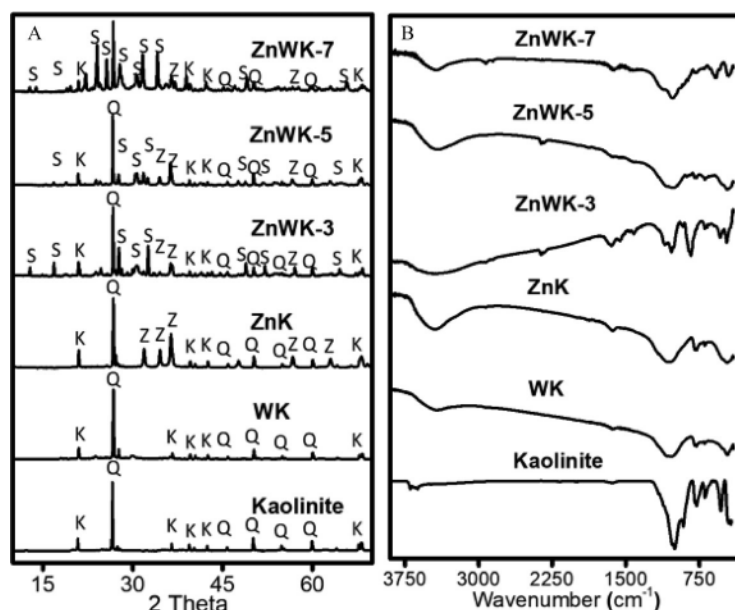
$$\% \text{ Removal} = \frac{C_o - C_f}{C_o} \times 100 \quad (2)$$

where  $C_o$  and  $C_f$  represent the initial and final contaminant concentrations, respectively. The time-dependent data were fitted to the Langmuir-Hinshelwood equation, based on a model commonly used for heterogeneous catalytic processes (34).

$$\ln\left(\frac{C_o}{C_t}\right) = k_{app}t \quad (3)$$

Where  $C_o$  and  $C_t$  are the concentrations of AMP in solution at time zero and at time  $t$ , respectively.  $k_{app}$  is the slope of the linear plot of  $\ln\left(\frac{C_o}{C_t}\right)$  against time  $t$ . The corresponding half-life ( $t_{1/2}$ ) values were calculated according to

$$t_{1/2} = \frac{0.693}{k_{app}} \quad (4)$$



**Figure 1.** (A) X-ray diffractogram (XRD) and (B) Fourier transform infrared (FTIR) spectra of kaolinite,  $\text{Zn}(\text{CH}_3\text{CO}_2)_2/\text{kaolinite}$  (ZnK),  $\text{Na}_2\text{WO}_4/\text{Kaolinite}$  (WK),  $\text{Zn}(\text{CH}_3\text{CO}_2)_2/\text{Na}_2\text{WO}_4\text{-Kaolinite}$  calcined at  $300^\circ\text{C}$  (ZnWK-3), (E)  $\text{Zn}(\text{CH}_3\text{CO}_2)_2/\text{Na}_2\text{WO}_4/\text{Kaolinite}$  calcined at  $500^\circ\text{C}$  (ZnWK-5) and  $\text{Zn}(\text{CH}_3\text{CO}_2)_2/\text{Na}_2\text{WO}_4/\text{Kaolinite}$  calcined at  $700^\circ\text{C}$  (ZnWK-7) [K = kaolinite, Q = quartz, S = sanmartinite ( $\text{ZnWO}_4$ ) and Z =  $\text{ZnO}$ ].

The degree of mineralization in water with the prepared photocatalysts was determined via the measurement of the oxygen equivalent of the organic matter present in each sample, *i.e.* total organic carbon (TOC), using a Shimadzu TOC VCPH Analyzer (P/N 638-91062-33; S/N 39N42773). The % mineralization was calculated using the equation

$$\% \text{ Mineralization} = \frac{\text{TOC}_o - \text{TOC}_e}{\text{TOC}_o} \times 100 \quad (5)$$

where  $\text{TOC}_o$  and  $\text{TOC}_e$  refer to the initial and the final total organic carbon, respectively.

The inorganic photocatalytic degradation by-products ( $\text{SO}_4^{2-}$ ,  $\text{NO}_3^-$  and  $\text{NH}_4^+$ ) were determined using a Metrohm Ion Chromatography system (Model 850) equipped with an electrical conductivity detector. An eluent mixture of 3.2 mM sodium carbonate/1.0 mM sodium bicarbonate eluents and a regenerating solution of 0.1 mM sulphuric acid were used for the determination of sulphate and nitrate anions while 1.7 mM nitric acid/0.7 mM dipicolinic acid eluent mixture was used for  $\text{NH}_4^+$  analysis.

## 2.4. Degradation products

Samples were subjected to liquid chromatography electrospray ionization mass spectrometry (LC-ESI-MS) LCMS analysis to ascertain the organic degradation products using an LTQ orbitrap Velos (Thermo Scientific)

interfaced with a Thermo Scientific UHPLC system equipped with an Accela 1250 pump. Sample separation was achieved on a C-18 column. An Agilent LC-MS fitted with a C-18 column was used. The following conditions were used in the analysis:

<b>Flow rate</b>	0.2 mL/min		
<b>Gradient method</b>	A – 95% $\text{H}_2\text{O}$ , 5% Acetonitrile, and 0.1% Formic acid B – 95% Acetonitrile, 5% $\text{H}_2\text{O}$ , and 0.1% Formic acid.		
<b>Programme</b>	Time	Mobile phase A (%)	Mobile phase B (%)
	0	100	0
	3	100	0
	27	40	60
	37	10	90
<b>ESI Ionization Mode:</b>	Positive and negative electrospray ionization mode		
<b>Mass range</b>	50–500 m/z		

## 2.5. Toxicity of treated water

The toxicity of the treated water was examined using the agar well diffusion method according to previously reported protocol (35). Aliquots from treated and untreated water contaminated with AMP were tested for change in toxicity against a gram-negative (*Escherichia coli* DSM 10974) and a gram-positive (*Staphylococcus aureus* ATCC 25923) bacteria. For this purpose, the entire surface of an agar plate was inoculated by spreading *E. coli* or *S. aureus* on it. Then, a hole with a diameter of ~6 mm was punched into the agar and 60  $\mu\text{L}$  of solution of treated and untreated AMP contaminated



water were introduced into the wells. The agar plate was incubated at 37°C overnight to promote the formation of inhibition zones around the wells.

## 2.6. Effects of some process variables

The effects of some process variables on the photocatalytic degradation of AMP using 100 mg/L ZnWK-5 composite (being the composites with the best efficiency) were studied. This includes the effect of initial concentration (25, 50 and 100 mg/L) using of 100 mg/L of the composite, the effect of photocatalyst dose (10, 20 and 50 mg) using 50 mg/L of AMP, the effect of pH (3.0, 5.0, 7.0, 9.0 and 11.0 adjusted with 0.1 M HCl and 0.1 M NaOH) using 50 mg/L AMP, and influence of inorganic anions ( $\text{Cl}^-$ ,  $\text{NO}_3^-$ ,  $\text{HCO}_3^-$ ,  $\text{SO}_4^{2-}$ , and  $\text{PO}_4^{3-}$ ) using 50 mg/L AMP. All studies were done using 100 mg/L of ZnWK-5 except when the photocatalyst dose was investigated. The reactive species generated during the photocatalytic process were investigated using 1 mmol L<sup>-1</sup> benzoquinone, 0.1 mL isopropyl alcohol and 1 mmol L<sup>-1</sup> sodium oxalate as scavengers to capture superoxide radical ( $\text{O}_2^-$ ) hydroxyl radical ( $\text{OH}^\cdot$ ) and holes, respectively.

## 2.7. Disinfection studies

In order to determine the potential of ZnWK-5 photocatalytic composite for the disinfection of water, 1 mL of 0.5 McFarland standard ( $1.5 \times 10^8$  cells) each of gram-positive bacteria [*Bacillus cereus* (ATCC10876) and *Staphylococcus aureus* (ATCC25923)] and gram-negative bacteria [*Escherichia coli* (DSM10974) and *Salmonella typhi* (ATCC13311)] were dispensed into 50 mL of sterile distilled water containing 10 mg of ZnWK-5 in sterile transparent flasks with continuous agitation under sunlight for 2 h. Aliquots (20  $\mu\text{L}$ ) of the contaminated water were withdrawn for analysis before and after the treatment process and analyzed using the pour plate method that involves the use of Mueller Hinton Agar incubated at 37°C for 24 h. To establish the impact of sunlight on the disinfection process, similar experiment (control) was repeated in the absence of ZnWK-5 photocatalyst. The plates were observed for inhibition of test organisms.

## 3. Results and discussion

### 3.1. Characterization

#### 3.1.1. X-ray diffraction (XRD)

The X-ray diffraction (XRD) pattern of kaolinite clay and the synthesized composite materials are shown in Figure 1(A). On the kaolinite diffractogram (Figure 4),

the mineral phases of anorthic kaolinite are observed at 12.5°, 20.1°, 36.7°, 40.4°, and 44.3° (ICSD 16597). Quartz peaks are located at  $2\theta = 26.7^\circ$ , 39.5°, 45.7°, 50.0°, 54.9°, 63.9°, and 68.2° (ICSD 67121). There is no significant difference between the XRD patterns of WK ( $\text{NaWO}_4 \cdot 2\text{H}_2\text{O}$  + kaolinite) composite and that of kaolinite (Figure 1). This is indicative of the fact that there was no formation of a new mineral phase contrary to expectations. However, for ZnK ( $\text{Zn}(\text{CH}_3\text{CO}_2)_2$  + kaolinite) diffractogram, new peaks suggesting the presence of ZnO mineral phases were observed at  $2\theta = 31.83^\circ$ , 34.65° and 36.32° and 62.98° (ICSD 157132) alongside those peaks unique for kaolinite phase.

The ZnWK composites ( $\text{NaWO}_4 \cdot 2\text{H}_2\text{O}$  +  $\text{Zn}(\text{CH}_3\text{CO}_2)_2$  + kaolinite) showed reflections of the mineral phases (kaolinite, quartz, and ZnO) earlier identified in the kaolinite and ZnK diffractograms. In addition, reflections stemming from monoclinic  $\text{ZnWO}_4$  (a sanmartinite phase) were observed at  $2\theta$  values of 15.5° (101), 18.8° (100), 23.7° (011), 30.62° (111), 31.3° (−111), 36.3° (021), 38.4° (120), 40.4° (200), 41.3° (−121), 48.8° (030) and 57.8° (212) (ICSD 84540) (36, 37). These new peaks confirm the incorporation of ZnO and  $\text{ZnWO}_4$  into kaolinite during the preparation of the composites. However, as expected, the peaks for the various composites are more distinct with increase in calcination temperature from 300°C to 700°C (Figure 1(A)) due largely to better defined crystallographic arrangement in the different mineral phases and the development of larger crystallite sizes as temperature increases (38).

#### 3.1.2. Fourier Transformed Infrared Spectroscopy (FTIR)

Figure 1(B) shows attenuated total reflectance-Fourier transform infrared (ATR-FTIR) spectra of Kaolinite, and prepared composites. The ATR-FTIR spectra of the raw Kaolinite exhibit bands that are assigned to anti-symmetric and symmetric stretching mode of  $-\text{O}-\text{H}$  between 3699 and 3618  $\text{cm}^{-1}$  (39). The  $-\text{O}-\text{H}$  bending vibrations of absorbed water are observed to be at 1636  $\text{cm}^{-1}$  (40). Bands at 1015 and 910  $\text{cm}^{-1}$  correspond to the Si–O and Al–OH in-plane bending vibrations, respectively (41). The peak at 779  $\text{cm}^{-1}$  is due to Si–O–Si inter-tetrahedral bridging bonds in the kaolinite (39). The peaks between 750 and 300  $\text{cm}^{-1}$  are M–O stretching vibrations (39). The bands at 785 and 690  $\text{cm}^{-1}$  were Si–O symmetric stretching while that at 535  $\text{cm}^{-1}$  indicates the Si–O–Al vibrations, where the Al is in octahedral coordination (42). The Fourier Transformed Infrared (FTIR) spectra of all composite materials (Figure 1(B)) show clear similarities in their spectrum with broad and distinct  $-\text{O}-\text{H}$  stretching and bending vibrations centered around 3328  $\text{cm}^{-1}$  and at

$1629\text{ cm}^{-1}$ , respectively, as well as the vibrations corresponding to Si–O and Al–OH (43) indicating the presence of kaolinite. The bending vibration of Zn–W–O, stretching vibration of W–O bond and symmetrical vibrations of bridge oxygen atoms of Zn–O–W groups from sanmartinite are observed at 763, 690, 648 and  $465\text{ cm}^{-1}$ , respectively (44, 45).

### 3.1.3. Scanning electron microscopy (SEM) and energy-dispersive X-ray (EDX) analysis

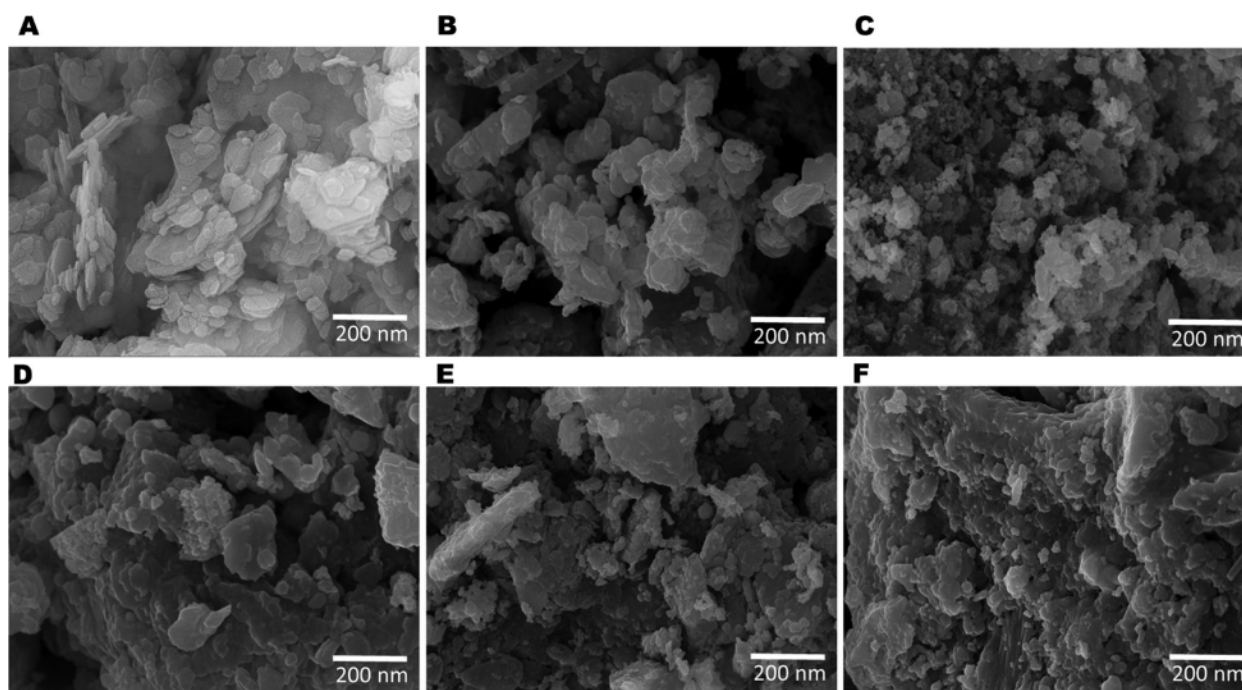
The Scanning Electron Microscope image of pure kaolinite reveals a morphology that suggests that the particles are packed in sheet-like form (Figure 2(A)). For the composites WK, ZnK and the zinc tungstate-kaolinite composites (ZnWK-3, ZnWK-5, and ZnWK-7), the particles are densely packed (Figure 2(B–F)).

The level of agglomeration increased with increase in calcination temperature especially with ZnWK-7 composite (Figure 2(F)). The densely agglomerated nature of the composite could be linked to the high calcination temperatures used during sample preparation (2). The SEM image of raw kaolinite (Figure 2(A)) shows the kaolinite sheet, meanwhile, this sheet-like structure is not observed for the prepared composites (Figure 2(B–F)) due to thermal treatment. The shapes and sizes of the particles of all the materials prepared are irregular and heterogeneously distributed. The Energy Dispersive X-

ray analysis of the composites (Table 1) show elements that confirm the presence of kaolinite, quartz, sanmartinite ( $\text{ZnWO}_4$ ) and ZnO minerals in the composites. As expected, the presence of the precursors in each of the prepared composites was indicated by the corresponding elements. However, K, Ti and Fe were observed in all the prepared composites as impurities in the natural kaolinite used as the support for the photocatalyst composites. Ti and Fe impurities have also been reported to impact positively on the photocatalytic activities of semiconductor photocatalyst (8).

### 3.1.5. UV/Vis diffuse reflectance spectroscopy (UV-DRS)

All composites show absorption in the visible light region (Figure 3(A)). This type of absorption is typical of oxygen vacancy and surface defects in materials. The UV/Vis absorption spectra and the apparent bandgap of the composites estimated from Tauc plot (33) are presented in Figure 3(A). The absorption spectra show that the prepared composites are visible light active. The apparent bandgaps  $E_g$  estimated using Tauc plot indicate an increase from 1.7 to 2.4 and to 2.5 for ZnWK-3, ZnWK-5 and ZnWK-7 composites, respectively (Figure 3(B)). This is similar to the observation in previous studies where increase in calcination temperature of the prepared ZnO photocatalytic



**Figure 2.** Scanning electron micrograph (SEM) of (A) kaolinite, (B)  $\text{Zn}(\text{CH}_3\text{CO}_2)_2/\text{kaolinite}$  (ZnK), (C)  $\text{Na}_2\text{WO}_4/\text{Kaolinite}$  (WK), (D)  $\text{Zn}(\text{CH}_3\text{CO}_2)_2/\text{Na}_2\text{WO}_4\text{-Kaolinite}$  calcined at  $300^\circ\text{C}$  (ZnWK-3), (E)  $\text{Zn}(\text{CH}_3\text{CO}_2)_2/\text{Na}_2\text{WO}_4/\text{Kaolinite}$  calcined at  $500^\circ\text{C}$  (ZnWK-5) and (F)  $\text{Zn}(\text{CH}_3\text{CO}_2)_2/\text{Na}_2\text{WO}_4/\text{Kaolinite}$  calcined at  $700^\circ\text{C}$  (ZnWK-7).

nanoparticles caused an increase in bandgap (46). This is related to the drop in quantum yield efficiency as a result of the reduction in the available surface area for photo-absorption for the generation of electron-hole pair ( $e^-$  to  $h^+$ ) (47).

### 3.1.6. Photoluminescence spectroscopy

The photoluminescence (PL) spectra of the synthesized composites indicate a blue-green broad emission (380–550 nm) spectra (Figure 3(C)) centered at *ca.* 430 nm. This kind of emission from ZnWK and WK photocatalyst composites is linked to the intrinsic emission of  $WO_6^{6-}$  complexes in  $ZnWO_4$ , where  $WO_6^{6-}$  octahedral act as luminescence center in the matrix with charge transfer occurring between the empty 4d W orbitals and the 2p O orbitals (48). The spectra represent typical photocatalytic systems in which relaxation involves the participation of numerous electronic states (49) and suggests that the composites are active emitters in the visible light region. This supports the UV/Vis results obtained in Figure 3(A). Meanwhile, the peak observed for ZnK and kaolinite can be linked to the ability of natural kaolinite to exhibit semiconducting property and strong oxygen adsorption since the kaolinite clay used was obtained from the natural environment (22). Even when the kaolinite was calcined, it still exhibited some fluorescence properties although, it was concluded that the main function of the kaolinite clay in the composite was as a substrate (2). Similarly, the spectra for ZnK and WK composites reveal that they are also active emitters in the visible light region. Evidence of this is seen in a later study in this work (Figure 6) where these materials show the capacity to photodegrade AMP in solution under sunlight irradiation.

**Table 1.** Energy-dispersive X-ray (EDX) analysis for spectra of kaolinite,  $Zn(CH_3CO_2)_2$ /kaolinite (ZnK),  $Na_2WO_4$ /Kaolinite (WK),  $Zn(CH_3CO_2)_2$ / $Na_2WO_4$ -Kaolinite calcined at 300°C (ZnWK-3),  $Zn(CH_3CO_2)_2$ / $Na_2WO_4$ /Kaolinite calcined at 500°C (ZnWK-5) and  $Zn(CH_3CO_2)_2$ / $Na_2WO_4$ /Kaolinite calcined at 700°C (ZnWK-7).

Element	Kaolinite <sup>a</sup>	ZnK	WK	ZnWK-3	ZnWK-5	ZnWK-7
O	42.52	57.48	60.40	60.86	54.82	57.85
Na	–	–	4.87	4.67	4.09	4.20
Al	23.90	6.79	6.48	6.18	6.27	5.36
Si	58.30	21.99	24.18	19.45	19.65	19.53
K	1.40	0.77	0.73	0.67	0.62	0.63
Ti	1.18	0.40	0.80	0.42	0.38	0.36
Fe	5.43	1.90	1.56	0.74	1.20	0.86
Zn	–	11.47	–	4.46	11.63	8.88
W	–	–	0.98	2.56	1.34	2.33

Note: The amounts are expressed in atomic percent composition of each atom in the composites.

<sup>a</sup>Data for kaolinite was abstracted from previous report by Unuabonah et al. (39).

### 3.1.7. Electron paramagnetic resonance

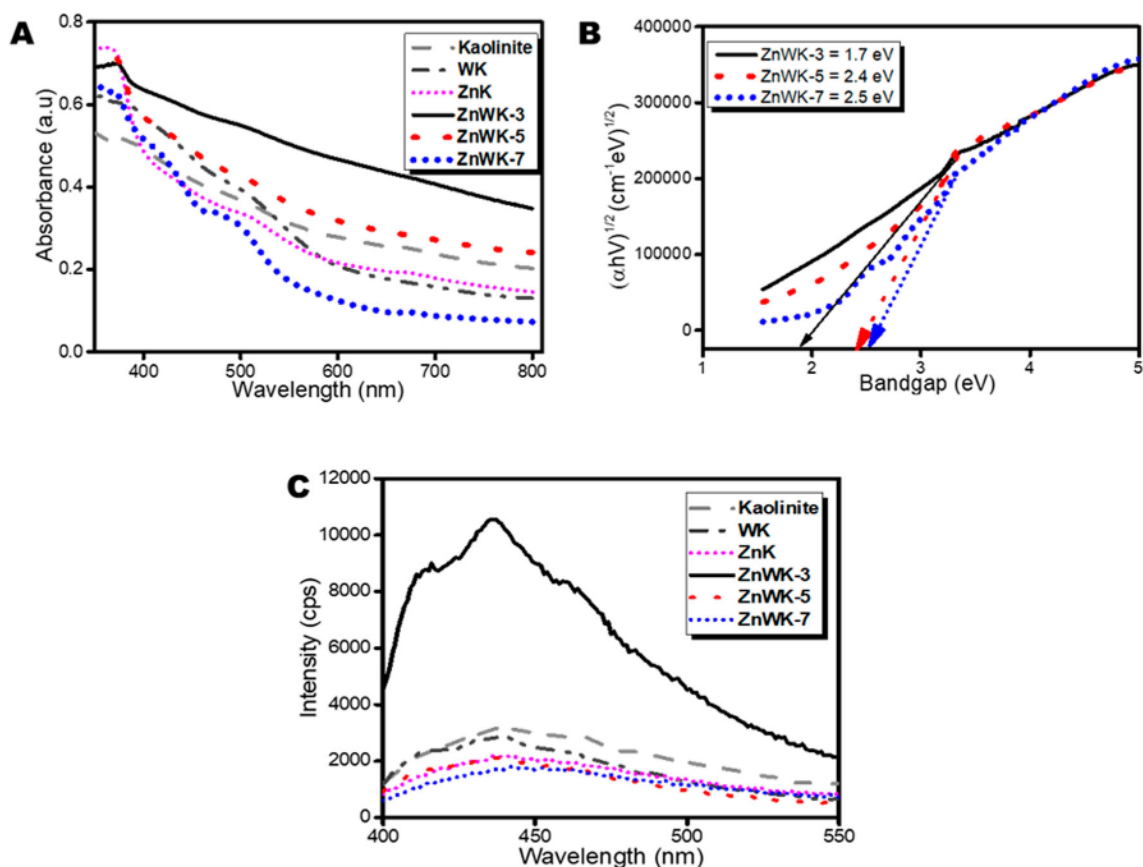
Further insights into the photochemical property of ZnWK-5 composite (being the most efficient composite material) is seen from the X-band EPR spectra shown in Figure 4. An intense sharp line near  $g=2.0034$  observed in the composite signifies unpaired electrons associated with carbon in the photocatalytic composite (8). The peak at  $g=2.0950$  suggests the presence of  $W^{5+}$  ions, attributed to surface defects in the crystal lattice of  $ZnWO_4$  (50). The  $W^{5+}$  species create defect levels below the conduction band that allows the photocatalytic composite to absorb light in the visible region of the electromagnetic spectrum. Furthermore, the  $W^{5+}$  species are known to enhance the separation efficiency of  $e^-$  and  $h^+$  pairs that ultimately end up increasing the photocatalytic activity of the composite (51). The peak at  $g=4.25$  arises from the presence of  $Fe^{3+}$  used in the preparation of the composite for EPR analysis.

### 3.1.8. X-ray photoelectron spectroscopy

The elemental composition and the corresponding valence states of the most efficient photocatalytic composite, ZnWK-5, were further studied with X-ray photoelectron spectroscopy (XPS). The survey spectra confirm the presence of Al, Si, Zn O, C, and W in the photocatalytic composite (Figure 5(A)) as earlier observed in the EDX analysis (Table 1). The presence of the C-atom confirms the successful doping of carbon into the composite via the zinc acetate precursor used for the synthesis. This is true because it has been confirmed that the kaolinite used in this study has no carbon in it (52). Figure 5(B) shows the high-resolution XPS spectrum of Zn 2p with decomposed peaks at 1020.8 and 1044.1 eV attributed to the Zn 2p<sub>3/2</sub> and Zn 2p<sub>1/2</sub> states of  $Zn^{2+}$  in the  $ZnWO_4$  component of the composite (53).

The binding energies at 34.5 and 36.4 eV, as shown in Figure 5(C) correspond to 4f<sub>7/2</sub> and 4f<sub>5/2</sub> spins of W also indicative of the presence of  $W^{5+}$  (54) confirming the earlier EPR results in this study. In addition, two small satellite peaks appeared at 35.4 eV for W 4f<sub>7/2</sub> orbit and 37.5 eV for W 4f<sub>5/2</sub>, further confirming the presence of W in the composite (55, 56). However, in these two satellite peaks of W, the intensity of  $W^{5+}$  is higher than for  $W^{6+}$  (Figure 5(C)), suggesting a higher amount of  $W^{5+}$  in the composite than  $W^{6+}$ . This  $W^{5+}$  defect state is known to have a strong relationship with oxygen vacancies (51, 57, 58) and enhances photocatalytic activity (51, 59). The O 1s high-resolution spectra are deconvoluted into two peaks located at 530.4 and 532.1 eV (Figure 5(D)), representing metal-oxygen bond which could be present as W–O and Zn–O

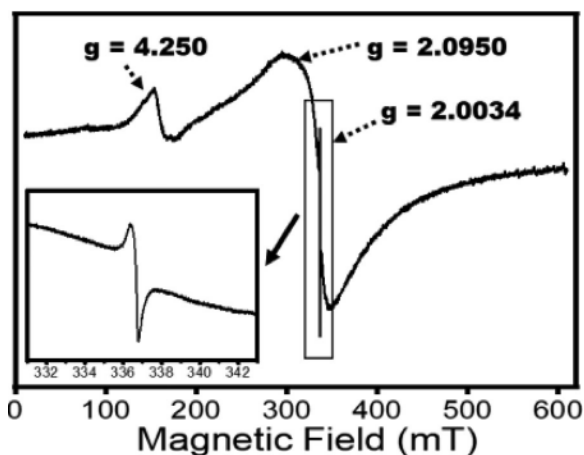




**Figure 3.** (A) Absorption spectra, (B) Tauc plots and (C) photoluminescence spectra (at the excitation wavelength of 380 nm) of kaolinite,  $\text{Zn}(\text{CH}_3\text{CO}_2)_2/\text{kaolinite}$  (ZnK),  $\text{Na}_2\text{WO}_4/\text{Kaolinite}$  (WK),  $\text{Zn}(\text{CH}_3\text{CO}_2)_2/\text{Na}_2\text{WO}_4\text{-Kaolinite}$  calcined at  $300^\circ\text{C}$  (ZnWK-3),  $\text{Zn}(\text{CH}_3\text{CO}_2)_2/\text{Na}_2\text{WO}_4/\text{Kaolinite}$  calcined at  $500^\circ\text{C}$  (ZnWK-5) and  $\text{Zn}(\text{CH}_3\text{CO}_2)_2/\text{Na}_2\text{WO}_4/\text{Kaolinite}$  calcined at  $700^\circ\text{C}$  (ZnWK-7).

(nanorod) in the composite (53, 56, 60). Two peaks are observed on the C 1s spectra (Figure 5(E)). The major peak at around 284.1 eV is attributed to the delocalized carbon (C–C bond) (61) within the composite, as a contribution from the Zinc acetate component precursor employed for the preparation of the composite. The

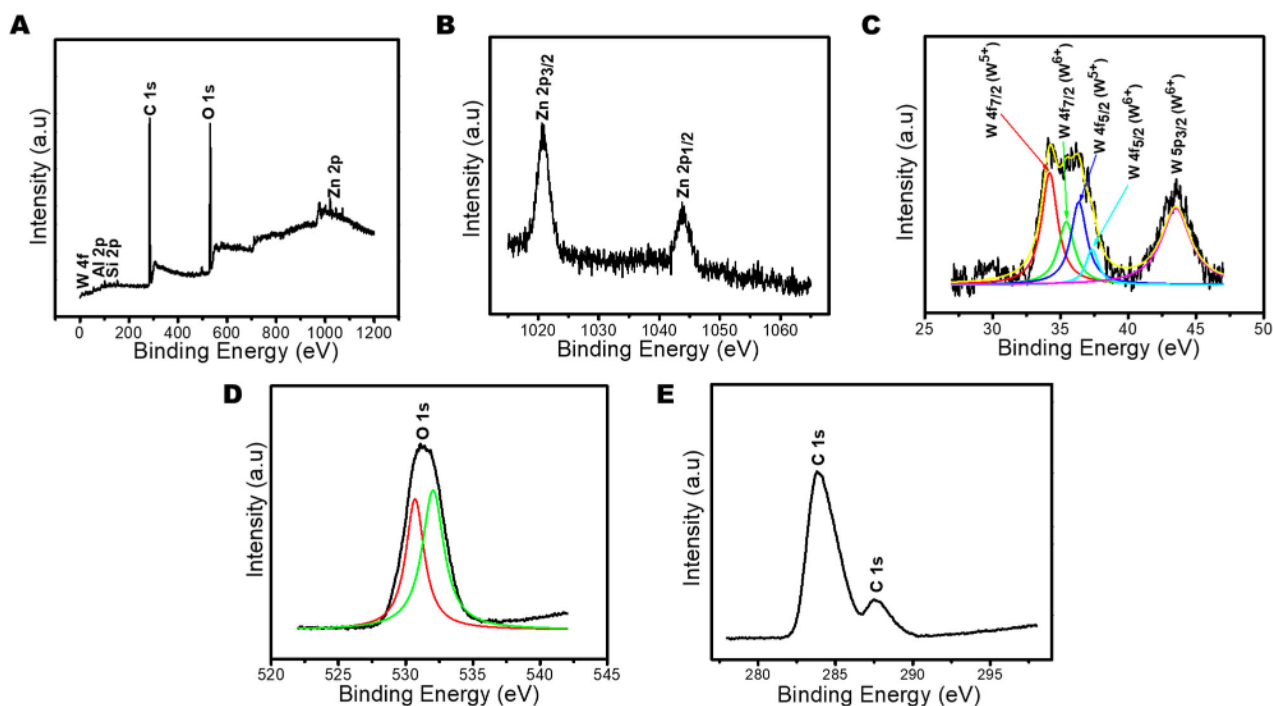
binding energies peak at 284.2 and 286.2 eV confirm the presence of  $\text{sp}^2$  carbon of C–H and C–O in the composite (Figure 5(E)) resulting from the use of carbon-rich Zn precursor in the photocatalysts preparation and C possibly from air contaminants (62). The presence of the C-atom confirms the successful doping of C into the composite via the zinc acetate precursor used for the synthesis.



**Figure 4.** X-band Electron Paramagnetic Resonance spectra of  $\text{Zn}(\text{CH}_3\text{CO}_2)_2/\text{Na}_2\text{WO}_4/\text{Kaolinite}$  photocatalytic composite (ZnWK-5) calcined at  $500^\circ\text{C}$ .

### 3.2. Removal of ampicillin in water

The prepared photocatalytic composites were screened for their adsorption and photocatalytic efficiency in removing AMP from water. The results show that photolysis alone (with 21% removal) does not have the capacity to sufficiently remove AMP from water within the time used in this experiment (Figure 6). However, photocatalytic degradation of AMP with kaolinite alone and with Tungstate-Kaolinite composite (WK) showed improved efficiencies of 47% and 44%, respectively. Nevertheless, with the introduction of zinc acetate to kaolinite and  $\text{Na}_2\text{WO}_4$  to form ZnO-K (ZnK) and ZnO-ZnWO<sub>4</sub> (ZnWK) composites, respectively, more AMP



**Figure 5.** X-ray photoelectron spectroscopy (XPS) (A) scan, (B) Zn 2p spectrum, (C) W 4f spectrum, (D) O 1s spectrum and (E) C 1s spectrum of  $\text{Zn}(\text{CH}_3\text{CO}_2)_2/\text{Na}_2\text{WO}_4/\text{Kaolinite}$  photocatalytic composite (ZnWK-5) calcined at  $500^\circ\text{C}$ .

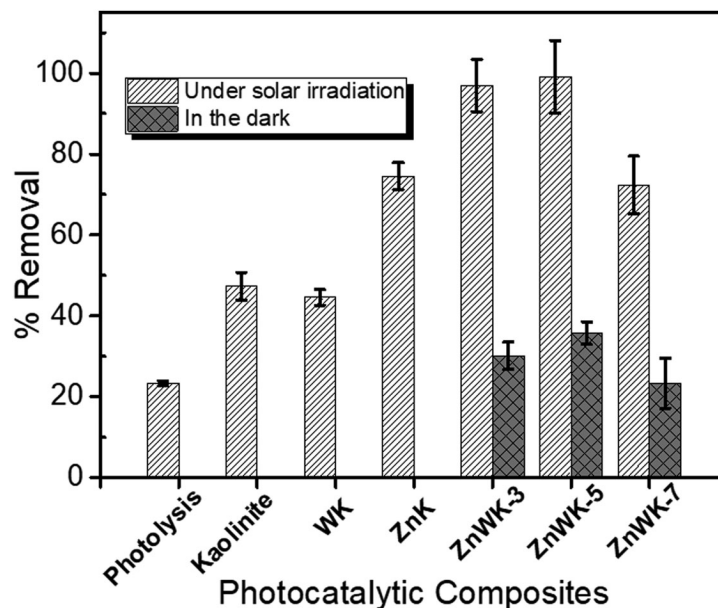
molecules were removed from aqueous solution (Figure 6). The  $\text{ZnO-ZnWO}_4$  (ZnWK) composites prepared at  $500^\circ\text{C}$  (ZnWK-5) gave the best efficiency of ca. 98% removal of AMP from aqueous solution (Figure 6).

Based on these results, the focus of this study is now on evaluating further, the efficiency of the most efficient

photocatalytic composites (ZnWK-5) for removal of AMP molecules in water.

### 3.2.1. Rate of ampicillin removal

The data for the time-dependent photodegradation of AMP molecules in water was analyzed further using



**Figure 6.** Photocatalysts screening with 50 mL of 50 mg/L Ampicillin under dark and solar irradiation for 120 min using 50 mg/L of kaolinite and the prepared composites.

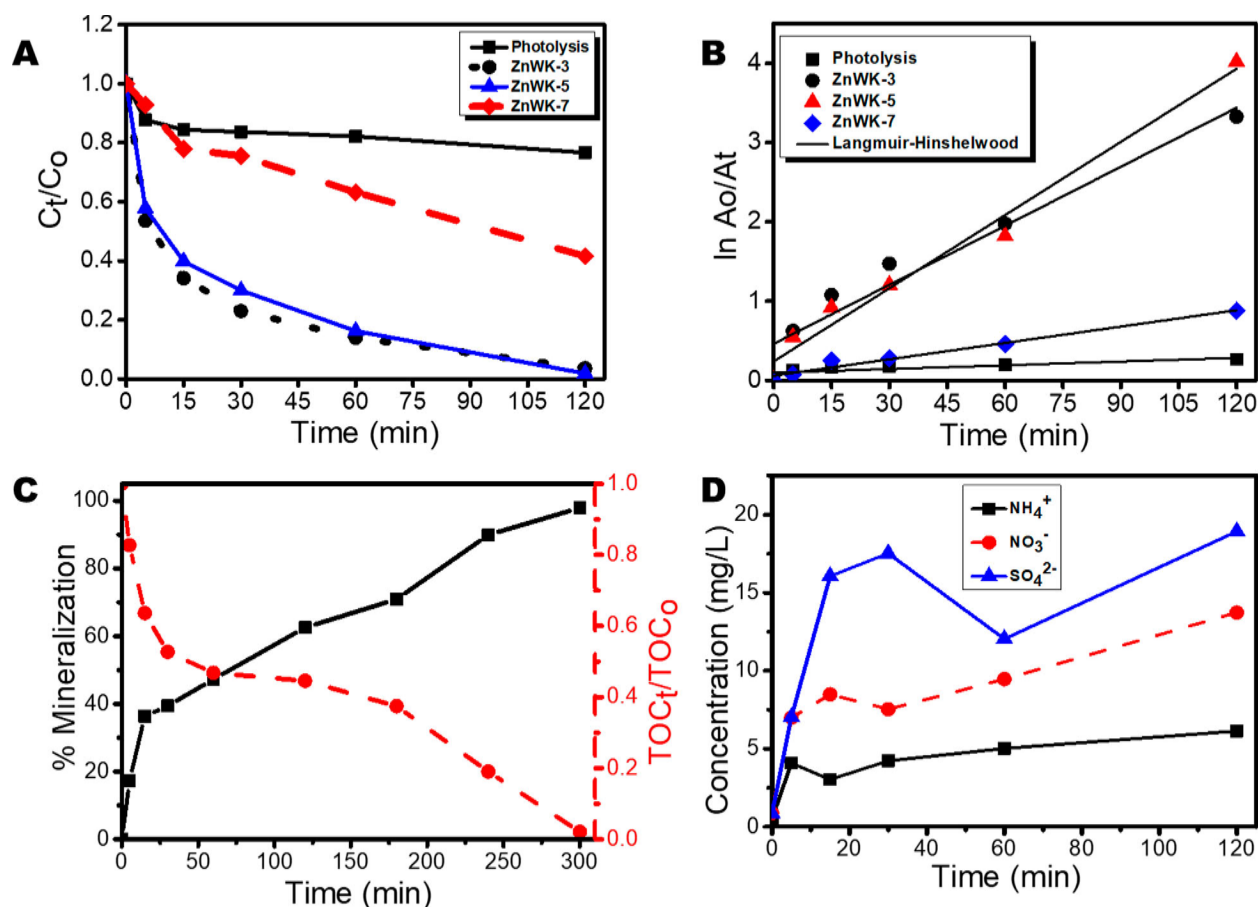
Langmuir–Hinshelwood (L-H) kinetic model (Figure 7(A, B)). The parameters in Table 2 show that the data fit the L-H kinetic model, suggesting that the photodegradation of AMP molecules on ZnWK-5 composite is a surface reaction and is a first-order kinetic process (63) dependent only on time and not on the concentration of AMP molecules. The L-H model parameters,  $k_{app}$  and  $t_{1/2}$ , reflect the fast removal rate constants for AMP (Table 2). Again, judging from the values of  $k_{app}$  obtained from L-H model (Table 2), the rate of removal of AMP molecules by ZnWK-5 composite is higher than those for ZnWK-3 composite and about 5 times higher than ZnWK-7 composite. This clearly supports our earlier inference that optimum calcination for the preparation of this composite is at 500°C. The rate of AMP removal by ZnWK-5 photocatalytic composite in this study ( $0.0308 \text{ min}^{-1}$ ) is much higher than those for P25 Degussa,  $0.0102 \text{ min}^{-1}$  (64);  $\text{Ru}/\text{WO}_3/\text{ZrO}_2$ ,  $0.0173 \text{ min}^{-1}$  (65), and  $\text{UV}/\text{ZnO}$ ,  $0.015 \text{ min}^{-1}$  (66).

The mineralization data in terms of TOC removal (Figure 7(C)) shows an essentially complete

**Table 2.** Kinetic parameters for the photodegradation of ampicillin (AMP).

Materials	$k_{app} (\text{min}^{-1})$	$t_{1/2} (\text{min})$	$r^2$	Std error
Photolysis	0.0016	433	0.5546	$5.8 \times 10^{-4}$
ZnWK-3	0.0248	28	0.9333	$2.9 \times 10^{-3}$
ZnWK-5	0.0308	23	0.9735	$2.3 \times 10^{-3}$
ZnWK-7	0.0069	100	0.9701	$5.3 \times 10^{-4}$

mineralization (ca. 98% TOC removal) of AMP molecules after 300 min of photocatalytic degradation in the presence of ZnWK-5 composite (Figure 7(C)). When compared with other tungstate- and non-tungstate-based photocatalytic materials used in the removal of AMP molecules in water, there is a significant improvement in TOC removal using ZnWK-5 photocatalytic composite (approximately 98% TOC removal after 300 min of interaction). For example, Singh *et al* achieved ca. 20% photomineralization of 35 mg/L AMP molecules after 2 h using 60% $\text{WO}_3/\text{BiOCl}$  stacked on graphene sand and on chitosan (67). Another study showed that with fluorinated Zn ( $\text{OH}$ )<sub>2</sub> in a sonophotocatalyzed system,



**Figure 7.** (A) Time profile plot showing the removal of Ampicillin from water, (B) Langmuir-Hinshelwood (L-H) kinetic model plot for the removal of AMP in water, (C) mineralization of AMP in water in terms of TOC removal, and (D) Inorganic by-products (anions) from mineralization of AMP in water.

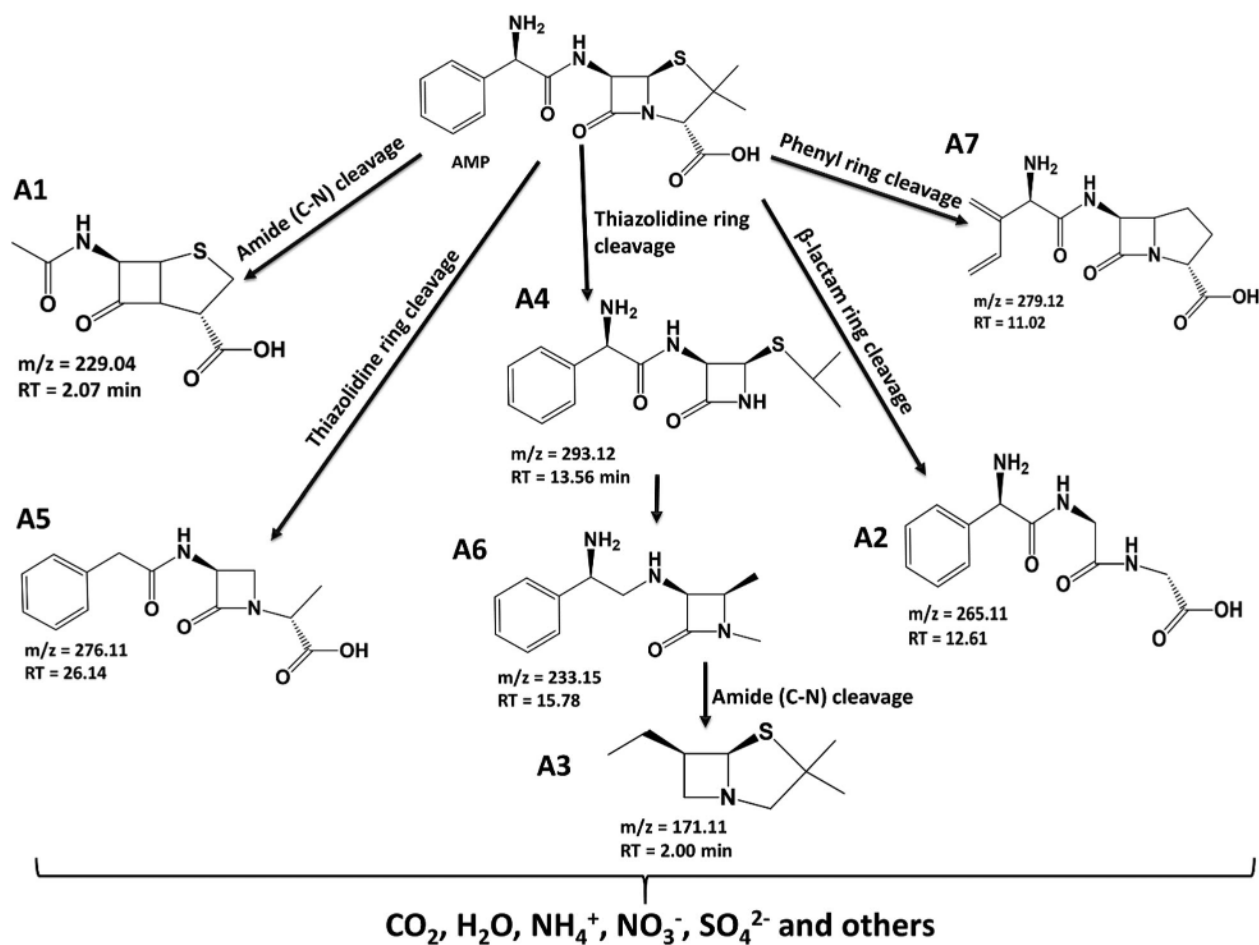
photomineralization of 30 mg/L of AMP molecules in water was 46% after 2 h (68). Though P25 degussa (a commercial photocatalyst) was reported to show a TOC removal of ca. 100% for AMP removal from water, this was achieved after 26 h using UV light (64) unlike 98% TOC removal in 300 min (5 h) under visible light as reported in this study.

### 3.3. Degradation product and proposed mineralization pathway

The release of anions during the photodegradation process further confirms the photo-mineralization of the AMP molecules by ZnWK-5 composite. The data for the inorganic anions generated during photodegradation of AMP molecules shows a very high yield of  $\text{SO}_4^{2-}$  compared with  $\text{NH}_4^+$  and  $\text{NO}_3^-$  (Figure 7(D)). This corroborates the mechanism of photodegradation as shown in the mass spectrometry analysis (Scheme 1), which suggests that the S-containing  $\beta$ -lactam ring serves as a major point of attack for the reactive species from the composite material

during the photocatalytic process. This indicates that the S-containing  $\beta$ -lactam ring is the most susceptible point of attack for reactive oxygen in the structure of an AMP molecule. This is similar to the observation in our previous study, where there was an unusually higher yield of  $\text{SO}_4^{2-}$  compared with N-based anions (8). However, the concentration of these anions in treated solution are well below their maximum concentration limits for drinking water ( $\text{SO}_4^{2-} = 250 \text{ mg/L}$ ,  $\text{NO}_3^- = 50 \text{ mg/L}$ ,  $\text{NH}_4^+ = 35 \text{ mg/L}$ ) as set by the World Health Organization standard guidelines (69) inspite of the high concentration of AMP (50 mg/L) used in this study.

The degradation products identified via ESI-LC-MS analysis and the proposed mineralization pathway for the degradation of AMP molecule are presented in Scheme 1. Based on the intermediates obtained, it is proposed that the degradation of AMP molecule using ZnWK-5 photocatalytic composite follows several steps. One of such step is the amide (C-N) bond cleavage of the AMP molecule to obtain compound A1 ( $m/z = 229.04$ ). On the other hand, the reactive species (from



**Scheme 1.** Degradation products for the degradation of ampicillin using  $\text{Zn}(\text{CH}_3\text{CO}_2)_2/\text{Na}_2\text{WO}_4/\text{Kaolinite}$  photocatalytic composite (ZnWK-5) calcined at  $500^\circ\text{C}$ .



the photocatalytic materials:  $h^+$ ,  $HO^\cdot$ ,  $^{\cdot}O_2^-$ ) attack the thiazolidine ring in the structure of AMP molecule to yield compounds A4 ( $m/z = 293.12$ ).

In addition, there is breakdown of the AMP molecule via the attack of the  $\beta$ -lactam ring to form compound A2 ( $m/z = 265.11$ ) and via phenyl ring cleavage to form A7 ( $m/z = 270.06$ ). Reduction of A4 ( $m/z = 293.12$ ) yields compound A6 ( $m/z = 233.15$ ), which is further decomposed to compounds A3 (207.06) and A8 ( $m/z = 171.11$ ) via the  $\beta$ -lactam ring cleavage, opening of its phenyl and thiazolidine rings respectively. There is also a  $\beta$ -lactam ring cleavage of AMP molecule to form compound A5 ( $m/z = 276.11$ ). The compounds formed are then further mineralized to  $CO_2$ ,  $H_2O$ ,  $NH_4^+$ ,  $NO_3^-$ , and  $SO_4^{2-}$  as revealed by the TOC and IC analysis of the supernatant solution of treated water (Figure 7(D)). The degradation data for all observed intermediates and the mass spectrum of each degradation product are presented in the supporting information document (Table S1).

### 3.4. Toxicity of treated water

The result from the analysis of the AMP-contaminated water before and after photomineralization with ZnWK-5 photocatalyst composite for the inhibition of *E. coli* DSM 10974 and *S. aureus* ATCC 25923 is presented in Figure 8. The result shows the zone of inhibition as a result of the presence of AMP molecule in solution before photocatalytic degradation experiment ( $14.50 \pm 0.71$  and  $10.75 \pm 0.35$  mm for *E. coli* and *S. aureus*, respectively). No zone of inhibition was observed for both *E. coli* and *S. aureus* after the photodegradation experiments. This suggests the loss of bacteria toxicity in treated solutions after the photodegradation of AMP-contaminated water with ZnWK-5 composite. This implies that the products of degradation are not toxic and no toxic matter is leached from ZnWK-5 composite into the treated water. By extension, this indicates the successful photomineralization of AMP in the

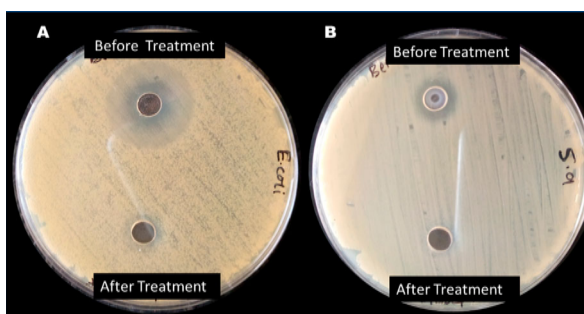
contaminated water by ZnWK-5 composite as corroborated by data from TOC analysis (Figure 7(C)). Therefore, it can be concluded that the application of ZnWK-5 composite for water treatment would help to reduce the development and spread of antibiotic-resistant bacteria (ARB) and antibiotic resistance genes (ARGs) among bacteria community in water.

### 3.5. Effects of some operational variables

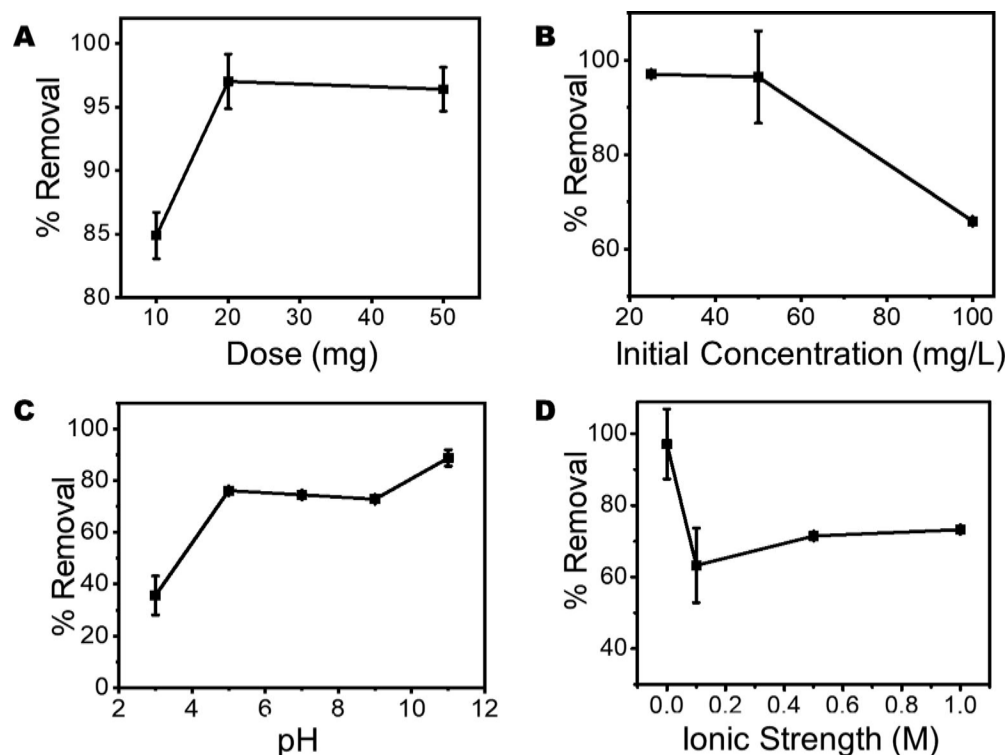
In the real world, water contains several other chemical species (aside pharmaceutical contaminants) and there are several operational variables that have the potential to alter the efficiency of a photocatalyst. To understand the impact of these chemical species and operational variables, this study considered the influence of five anions ( $Cl^-$ ,  $NO_3^-$ ,  $HCO_3^-$ ,  $SO_4^{2-}$ ,  $PO_4^{3-}$ ), pH, photocatalyst dose, initial concentration of AMP, and the change in ionic strength of the AMP solution. The results of the impact of varied photocatalyst dose at a fixed concentration of 50 mg/L of AMP (Figure 9(A)) shows that catalyst-to-substrate ratio plays important role in the photocatalytic degradation of AMP molecules in water. It is observed that an increase in the catalysts-to-substrate ratio is associated with an increase in the % removal of AMP molecules from the solution.

It has been reported that an increase in photocatalyst dose actually increases the number of active sites available for photocatalysis and hence increases the production of reactive radicals that enhance the efficiency of the photocatalyst (70).

However, in contrast to the effect of photocatalyst dose on the degradation of AMP molecules, it is observed that as the initial AMP concentration increases beyond 50 mg/L there is an observable decrease in the percentage removal of the pharmaceutical contaminant (Figure 9(B)). This is linked to the reduction in the photocatalyst to contaminant ratio that reduces the active photocatalytic sites available for photodegradation of AMP molecules in water (71, 72). However, increasing solution pH of AMP from 3.0 to 5.0 does increase the efficiency of ZnWK-5 composite to remove AMP molecules from an aqueous solution (Figure 9(C)). This efficiency is then maintained at comparable values between pH 5.0 and 9.0. Within this range of pH it is established from speciation studies that neutral species of AMP molecules are dominant (8, 73). This may explain the stable photocatalytic efficiency of ZnWK-5 composite exhibited within this range of pH during photocatalysis. However, at higher pH values ( $> 9.0$ ), the formation of hydroxyl radicals is encouraged, which strongly promotes photodegradation (21). The introduction of  $Na^+$  and  $Cl^-$  species to increase the



**Figure 8.** Result of toxicity test of (A) *Escherichia coli* DSM 10974 and (B) *Staphylococcus aureus* ATCC 25923 contaminated water before and after treatment with ZnWK-5 composite



**Figure 9.** Plots of the effect of change in (A) Photocatalyst dose at fixed AMP concentration, (B) initial AMP concentration at fixed catalyst dose, (C) AMP solution pH (D) Ionic strength of the AMP solution, on the photodegradation of 50 mg/L of the AMP in water.

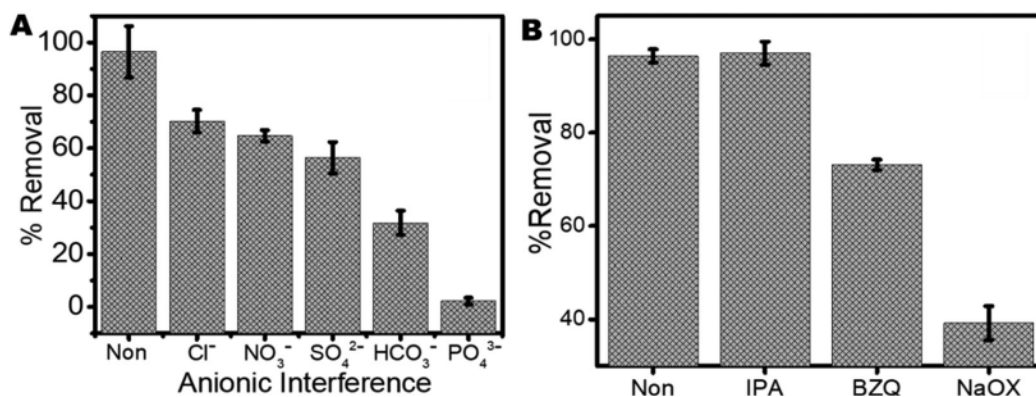
ionic strength of the solution reduces the photoactivity of ZnWK-5 photocatalyst but only improves its photoactivity only slightly as the ionic strength increases to 1.0 M (Figure 9(D)).

### 3.6. Effect of the presence of inorganic anion

In considering the influence of the presence of anions in AMP solution (Figure 10(A)), it is observed that all five anions ( $\text{Cl}^-$ ,  $\text{NO}_3^-$ ,  $\text{HCO}_3^-$ ,  $\text{SO}_4^{2-}$ ,  $\text{PO}_4^{3-}$ ) have a negative

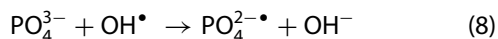
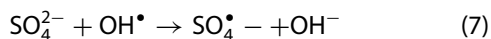
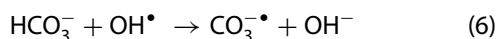
influence on the photocatalytic degradation of AMP molecules. The most negative impact is seen to be influenced by the presence of carbonate ( $\text{HCO}_3^-$ ) and phosphate ( $\text{PO}_4^{3-}$ ) anions. In several reports, this phenomenon is typical with these anions which are known to compete for photocatalytic sites with drug molecules (8).

These anions are known to scavenge reactive species in solution, thereby inhibiting their availability for the degradation of pharmaceutical contaminants in



**Figure 10.** The effect of (A) the presence of inorganic anions and (B) radical scavengers on the photodegradation efficiency of Ampicillin (AMP) molecules in water using ZnWK-5 composite (IPA = isopropyl alcohol, BZQ = benzoquinone and NaOX = sodium oxalate).

solution. Both  $\text{HCO}_3^-$  and  $\text{PO}_4^{3-}$  have been reported to be good scavengers of  $\text{HO}^\bullet$ , thereby limiting the roles of the photo-generated  $\text{HO}^\bullet$  for the degradation of target pharmaceutical contaminants according to Equations (6)–(8) (74, 75).

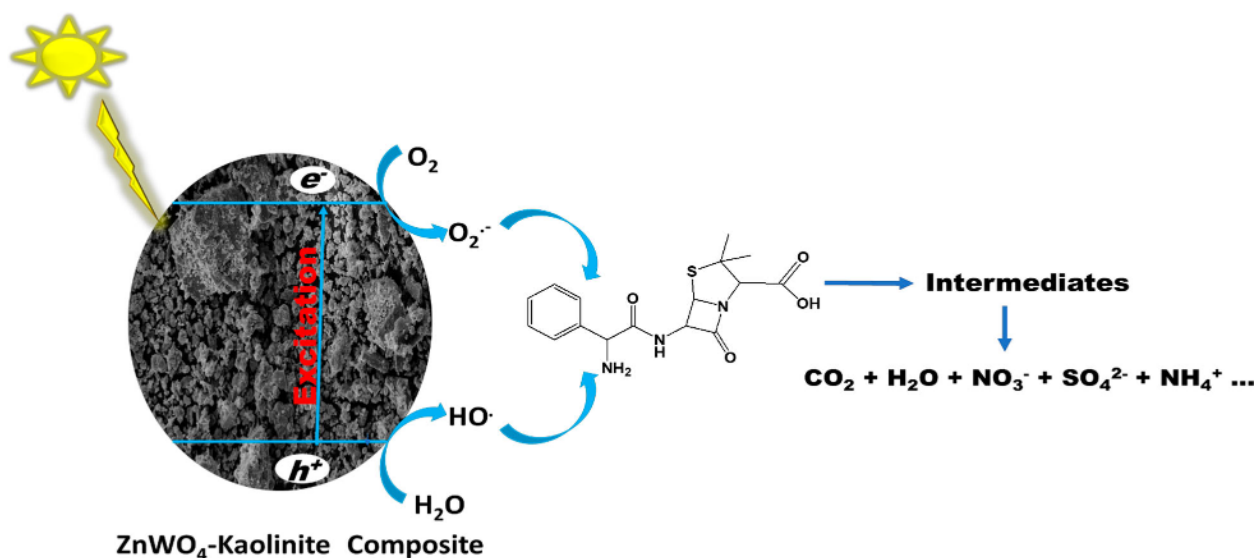
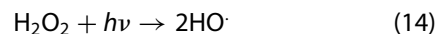
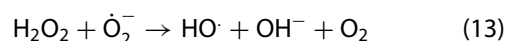
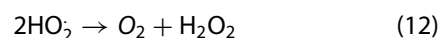
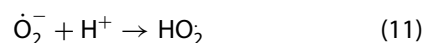
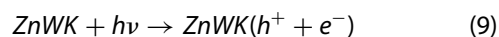


### 3.7. Reactive species responsible for photocatalytic degradation

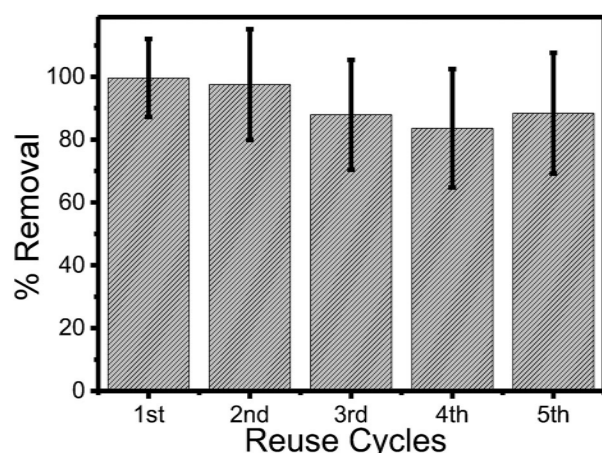
Several reactive species ( $\text{HO}^\bullet$ ,  $h^+$ ,  $\text{O}_2^{\bullet-}$ ,  $\text{O}_2$  etc) have been identified as being responsible for the photodegradation of organic molecules in solutions. However, not all of these reactive species are significantly involved in any photocatalytic process. To determine which of these reactive species were released by ZnWK-5 photocatalytic composite and played a significant role in the photodegradation of the AMP molecules, we used the scavenging effect method. Figure 10(B) shows the extent of scavenging by different chemicals: isopropanol (for  $\text{HO}^\bullet$ ), benzoquinone (for  $\text{O}_2^{\bullet-}$ ) and sodium oxalate (for  $h^+$ ). The presence of all scavenging chemicals decreased the photodegradation of AMP molecules, with  $h^+$  reactive specie being the most influenced. This suggests that the exposed hole ( $h^+$ ) plays a decisive role in the photocatalytic activity of ZnWK-5 composite while the superoxide anion radicals ( $\text{O}_2^{\bullet-}$ ) are the main

active species in the photocatalytic degradation of AMP molecules. However,  $\text{HO}^\bullet$  and  $\text{O}_2^{\bullet-}$  radicals are suggested to act in supplementary manner.

Equations (9)–(14) show the mechanistic approach for the generation of reactive species and the photodegradation of AMP molecules in solution based on the scavenger analysis. Generally, when the reaction medium is exposed to solar light, the solar irradiation of the composite transits electrons in the valence band of ZnWK to the conduction band to form electron–hole pairs. The  $h^+$  in the valence band oxidizes  $\text{H}_2\text{O}$  and  $\text{OH}^-$ . Meanwhile, the electron migrates to the surface of the photocatalyst and reacts with  $\text{O}_2$  to form  $\text{O}_2^{\bullet-}$ . Consequently, the  $\text{O}_2^{\bullet-}$  reacts with  $\text{H}^+$  and  $\text{H}_2\text{O}$  to form  $\text{HO}_2^\bullet$  and  $\text{H}_2\text{O}_2$ , respectively (equation p–q). While the  $\text{H}_2\text{O}_2$  further breaks down into  $\text{HO}^\bullet$  via the absorption of visible light energy (76). The reactive species produced, then initiate the degradation of AMP molecules in solution, as shown in Equations (9)–(14).



**Scheme 2.** Photodegradation scheme for the degradation of ampicillin in water by  $\text{Zn}(\text{CH}_3\text{CO}_2)_2/\text{Na}_2\text{WO}_4/\text{Kaolinite}$  photocatalytic composite (ZnWK-5) calcined at  $500^\circ\text{C}$ .



**Figure 11.** Stability of the efficiency of ZnWK-5 composite over five reuse cycles for the photodegradation of ampicillin (AMP) in water.

These reactive species produced in Equations (10), (13) and (14), then initiate the degradation of AMP molecules in solution as shown in Scheme 2.

### 3.8. Stability of photocatalytic composite

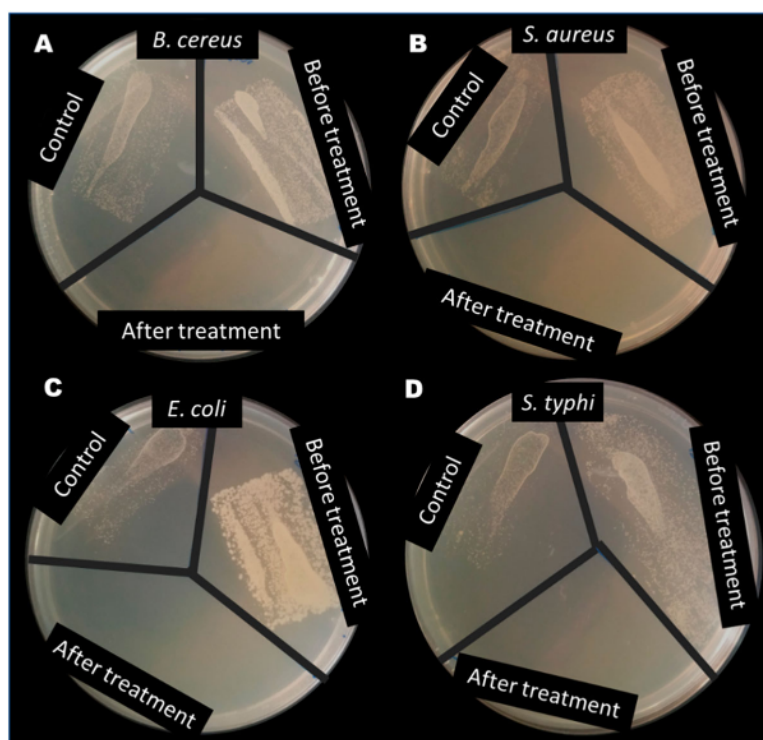
In considering upscaling the application of ZnWK-5 photocatalytic composite, it is important to establish its reusability over several cycles. The results for the reuse of ZnWK-5 photocatalytic composite for the

photodegradation of AMP molecules over a 5-cycle period are presented in Figure 11.

The ZnWK-5 photocatalytic composite demonstrates a high stability index of 100% after the first two reuse cycles for the removal of AMP from the solution. However, at the third reuse, about 10% loss in efficiency was observed, and this was sustained through to the fifth reuse cycle even though a slight increase in the photocatalytic efficiency was observed at the fifth reuse cycle. However, based on the error margins as shown in Figure 11, this difference has been considered not to be very significant especially after the third reuse. This shows that the semiconductors in the ZnWK-5 photocatalyst were properly anchored into the kaolinite clay support and its active surface is not significantly deactivated by the photodegradation process. The 10% loss in efficiency can be attributed to catalysts deactivation due to adsorbed substrates on their surfaces over several reuse cycles (77).

### 3.9. Water disinfection study

Aliquots of the treated water collected after the disinfection experiments (as described in section 2.7) were incubated for 24 h. The result showed that the exposure of the gram (+ve) bacteria (*Bacillus cereus* (ATCC10876) and *Staphylococcus aureus* (ATCC25923) and gram (–



**Figure 12.** Test result from disinfection of water containing (A) *B. Cereus*, (B) *S. aureus*, (C) *E. coli* and (D) *S. typhi* using ZnWK-5 photocatalytic composite.



ve) bacteria (*Escherichia coli* (DSM10974) and *Salmonella typhi* (ATCC13311) to sunlight (as control) only inhibited the growth of the bacteria slightly (Figure 12), this can be attributed to the UV component of the solar light spectrum of the study environment as reported in our previous study (19). However, the introduction of ZnWK-5 photocatalytic composite completely inhibited the growth of all bacteria studied (Figure 12), as there was no growth of these bacteria in the portions bearing the ZnWK-5 particles after 2 h of disinfection. The efficacy of the photocatalyst could be attributed to the presence of the superoxide radical ( $O_2^-$  as earlier suggested in section 3.7 (Figure 10(B)). This is consistent with previous reports for visible light photocatalytic disinfection of water (78, 79). It confirms that the prepared photocatalytic composite in this study is capable of disinfecting water contaminated with both gram (–ve) and gram (+ve) bacteria.

#### 4. Conclusion

A new heterogeneous photocatalytic composite with enhanced visible-light-induced photocatalytic degradation of ampicillin (AMP), was successfully prepared via a cheap and environmentally friendly mechano-thermal synthesis. Optical characterization of photocatalytic materials (prepared in this study) showed that the photo-activity of the  $ZnWO_4$ -kaolinite composites was due to the presence of  $W^{5+}$  defect states in the composite. Investigation showed that thermal treatment of the composite at 500°C (ZnWK-5 composite) provided a photocatalytic material that is more efficient for the mineralization of AMP molecules in water and disinfection of same. This photocatalytic composite showed a 98% photo-mineralization of 50 mg/L AMP molecules in water after 5 h. This, when compared with the photomineralization activity of commercial P25 degussa was far more efficient for the complete and safe removal of AMP from water. In addition, the same ZnWK-5 composite material was used to achieve total disinfection of water samples containing four bacteria (*E. coli*, *S. typhi*, *B. cereus*, *S. aureus*) under sunlight irradiation. However, in the presence of anions such as  $Cl^-$ ,  $NO_3^-$ ,  $PO_4^{3-}$ ,  $SO_4^{2-}$ , and  $HCO_3^-$  (which, at certain concentrations, are pollutants in water), the efficiency of the photocatalytic material reduced. This was more significant in the presence of  $PO_4^{3-}$ . Reuse studies with ZnWK-5 composite suggests that its efficiency is relatively stable even after five cycles. Overall, this study demonstrates that cheap raw materials combined with photoactive components provide viable access for the development of visible light photocatalytic composites suited for the

efficient removal of antibiotic chemicals and bacteria in water. Therefore, the application of ZnWK-5 for photomineralization water treatment would help to reduce the spread of antibiotics, development of antibiotics resistance bacteria (ARB) and transfer of antibiotics resistance genes (ARGs) among bacteria community in water.

#### Acknowledgement

The authors sincerely appreciate Prof Hellmut Eckert of the Sao Carlos Institute of Physics, University of Sao Paulo, Brazil for the analysis of the sample with Electron Paramagnetic Resonance, UV Vis spectroscopy equipment.

#### Disclosure statement

No potential conflict of interest was reported by the author(s).

#### Funding

E. I. U. and A. M. O. acknowledges, The World Academy of Sciences (TWAS) and the Brazilian National Council for Scientific and Technological Development (CNPq) for the TWAS-CNPq Sandwich PhD fellowship [grant number 315007/2018-4] to undertake this study. E. I. U. acknowledge with thanks the equipment grant from Alexander von Humboldt Foundation, Germany, for the purchase of Total Organic Carbon (TOC) equipment used in this study.

#### ORCID

Martins O. Omorogie  <http://orcid.org/0000-0001-9697-2960>

Emmanuel I. Unuabonah  <http://orcid.org/0000-0001-9854-3924>

#### References

- [1] Unuabonah, E.I.; Ugwuja, C.G.; Omorogie, M.O.; Adewuyi, A.; Oladoja, N.A. Clays for Efficient Disinfection of Bacteria in Water. *Appl. Clay Sci.* **2018**, *151*, 211–223.
- [2] Ugwuja, C.G.; Adelowo, O.O.; Ogunlaja, A.; Omorogie, M.O.; Olukanni, O.D.; Ikimiukor, O.O.; Iermak, I.; Kolawole, G.A.; Guenter, C.; Taubert, A.; Bodede, O.; Moodley, R.; Inada, N.M.; de Camargo, A.S.S.; Unuabonah, E.I. Visible-Light-Mediated Photodynamic Water Disinfection @ Bimetallic-Doped Hybrid Clay Nanocomposites. *ACS Appl. Mater. Interfaces* **2019**, *11*, 25483–25494.
- [3] Anthony, E.T.; Ojemaye, M.O.; Okoh, O.O.; Okoh, A.I. A Critical Review on the Occurrence of Resistomes in the Environment and Their Removal from Wastewater Using Apposite Treatment Technologies: Limitations; Successes and Future Improvement. *Environ. Pollut.* **2020**, *263*, 113791.
- [4] Nielsen, T.B.; Brass, E.P.; Gilbert, D.N.; Bartlett, J.G.; Spellberg, B. Sustainable Discovery and Development of Antibiotics—is a Nonprofit Approach the Future? *N. Engl. J. Med.* **2019**, *381*, 503.

- [5] Rizzo, L.; Manaia, C.; Merlin, C.; Schwartz, T.; Dagot, C.; Ploy, M.; Michael, I.; Fatta-Kassinos, D. Urban Wastewater Treatment Plants as Hotspots for Antibiotic Resistant Bacteria and Genes Spread Into the Environment: A Review. *Sci. Total Environ.* **2013**, *447*, 345–360.
- [6] Iwane, T.; Urase, T.; Yamamoto, K. Possible Impact of Treated Wastewater Discharge on Incidence of Antibiotic Resistant Bacteria in River Water. *Water Sci. Technol.* **2001**, *43*, 91–99.
- [7] Mahmood, A.R.; Al-Haideri, H.H.; Hassan, F.M. Detection of Antibiotics in Drinking Water Treatment Plants in Baghdad City, Iraq. *Adv. Public. Health.* **2019**, *2019*, 7851354.
- [8] Alfred, M.O.; Omorogie, M.O.; Bodede, O.; Moodley, R.; Ogunlaja, A.; Adeyemi, O.G.; Günter, C.; Taubert, A.; Iermak, I.; Eckert, H.; de Camargo, A.S.S.; Motheo, A.d.J.; Stuart, C.M.; Unuabonah, E.I. Solar-Active Clay-TiO<sub>2</sub> Nanocomposites Prepared via Biomass Assisted Synthesis: Efficient Removal of Ampicillin, Sulfamethoxazole and Artemether in Water. *Chem. Eng. J.* **2020**, *398*, 125544.
- [9] Blanset, D.L.; Zhang, J.; Robson, M.G. Probabilistic Estimates of Lifetime Daily Doses from Consumption of Drinking Water Containing Trace Levels of N, N-Diethyl-Meta-Toluamide (DEET), Triclosan, or Acetaminophen and the Associated Risk to Human Health. *Human Ecol. Risk Assess.* **2007**, *13*, 615–631.
- [10] Egbedina, A.O.; Adebawale, K.O.; Olu-Owolabi, B.I.; Unuabonah, E.I.; Adesina, M.O. Green Synthesis of ZnO Coated Hybrid Biochar for the Synchronous Removal of Ciprofloxacin and Tetracycline in Wastewater. *RSC Adv.* **2021**, *11*, 18483–18492.
- [11] Tran, N.H.; Chen, H.; Reinhard, M.; Mao, F.; Gin, K.Y.-H. Occurrence and Removal of Multiple Classes of Antibiotics and Antimicrobial Agents in Biological Wastewater Treatment Processes. *Water Res.* **2016**, *104*, 461–472.
- [12] Heberer, T.; Feldmann, D. Removal of pharmaceutical residues from contaminated raw water sources by membrane filtration. In *Pharmaceuticals in the Environment*; Kümmeler, K., Eds.; Springer, 2008, pp. 427–453.
- [13] Liu, M.-k.; Liu, Y.-y.; Bao, D.-d.; Zhu, G.; Yang, G.-h.; Geng, J.-f.; Li, H.-t. Effective Removal of Tetracycline Antibiotics from Water Using Hybrid Carbon Membranes. *Sci. Rep.* **2017**, *7*, 1–8.
- [14] Dolar, D.; Gros, M.; Rodriguez-Mozaz, S.; Moreno, J.; Comas, J.; Rodriguez-Roda, I.; Barceló, D. Removal of Emerging Contaminants from Municipal Wastewater with an Integrated Membrane System MBR–RO. *J. Hazard. Mater.* **2012**, *239–240*, 64–69.
- [15] Ensano, B.M.B.; Borea, L.; Naddeo, V.; Belgiorio, V.; De Luna, M.D.G.; Ballesteros, F.C. Removal of Pharmaceuticals from Wastewater by Intermittent Electrocoagulation. *Water* **2017**, *9*, 85.
- [16] Aldeguer Esquerdo, A.; Varo Galvañ, P.J.; Sentana Gadea, I.; Prats Rico, D. Carbamazepine and Diclofenac Removal Double Treatment: Oxidation and Adsorption. *Int. J. Environ. Res. Public Health* **2021**, *18*, 7163.
- [17] Mohapatra, D.P.; Brar, S.K.; Tyagi, R.D.; Picard, P.; Surampalli, R.Y. Analysis and Advanced Oxidation Treatment of a Persistent Pharmaceutical Compound in Wastewater and Wastewater Sludge–Carbamazepine. *Sci. Total Environ.* **2014**, *470*, 58–75.
- [18] Priya, B.; Shandilya, P.; Raizada, P.; Thakur, P.; Singh, N.; Singh, P. Photocatalytic Mineralization and Degradation Kinetics of Ampicillin and Oxytetracycline Antibiotics Using Graphene Sand Composite and Chitosan Supported BiOCl. *J. Mol. Catal. A: Chem.* **2016**, *423*, 400–413.
- [19] Alfred, M.O.; Omorogie, M.O.; Bodede, O.; Moodley, R.; Ogunlaja, A.; Adeyemi, O.G.; Günter, C.; Taubert, A.; Iermak, I.; Eckert, H. Solar-active Clay-TiO<sub>2</sub> Nanocomposites Prepared via Biomass Assisted Synthesis: Efficient Removal of Ampicillin, Sulfamethoxazole and Artemether from Water. *Chem. Eng. J.* **2020**, *398*, 125544.
- [20] Wang, H.; Zhang, J.; Yuan, X.; Jiang, L.; Xia, Q.; Chen, H. Photocatalytic Removal of Antibiotics from Natural Water Matrices and Swine Wastewater via Cu (I) Coordinately Polymeric Carbon Nitride Framework. *Chem. Eng. J.* **2020**, *392*, 123638.
- [21] Elmolla, E.S.; Chaudhuri, M. Comparison of Different Advanced Oxidation Processes for Treatment of Antibiotic Aqueous Solution. *Desalination* **2010**, *256*, 43–47.
- [22] Jiang, D.; Liu, Z.; Fu, L.; Jing, H.; Yang, H. Efficient Nanoclay-Based Composite Photocatalyst: The Role of Nanoclay in Photogenerated Charge Separation. *J. Phys. Chem. C* **2018**, *122*, 25900–25908.
- [23] Li, C.; Sun, Z.; Song, A.; Dong, X.; Zheng, S.; Dionysiou, D.D. Flowing Nitrogen Atmosphere Induced Rich Oxygen Vacancies Overspread the Surface of TiO<sub>2</sub>/Kaolinite Composite for Enhanced Photocatalytic Activity Within Broad Radiation Spectrum. *Appl. Catal., B* **2018**, *236*, 76–87.
- [24] Zyoud, A.H.; Zubi, A.; Zyoud, S.H.; Hilal, M.H.; Zyoud, S.; Qamhie, N.; Hajamohideen, A.; Hilal, H.S. Kaolin-supported ZnO Nanoparticle Catalysts in Self-Sensitized Tetracycline Photodegradation: Zero-Point Charge and pH Effects. *Appl. Clay Sci.* **2019**, *182*, 105294.
- [25] Babu, B.; Koutavarapu, R.; Shim, J.; Yoo, K. Enhanced Solar Light-Driven Photocatalytic Degradation of Tetracycline and Organic Pollutants by Novel one-Dimensional ZnWO<sub>4</sub> Nanorod-Decorated two-Dimensional Bi<sub>2</sub>WO<sub>6</sub> Nanoflakes. *J. the Taiwan Inst. Chem. Eng.* **2020**, *110*, 58–70.
- [26] Zhang, C.; Zhang, H.; Zhang, K.; Li, X.; Leng, Q.; Hu, C. Photocatalytic Activity of ZnWO<sub>4</sub>: Band Structure, Morphology and Surface Modification. *ACS Appl. Mater. Interfaces* **2014**, *6*, 14423–14432.
- [27] Bayode, A.A.; Vieira, E.M.; Moodley, R.; Akpotu, S.; de Camargo, A.S.; Fatta-Kassinos, D.; Unuabonah, E.I. Tuning ZnO/GO p-n Heterostructure with Carbon Interlayer Supported on Clay for Visible-Light Catalysis: Removal of Steroid Estrogens from Water. *Chem. Eng. J.* **2020**, *420*, 127668.
- [28] Derisso, C.R.; Pompei, C.M.E.; Spadoto, M.; da Silva Pinto, T.; Vieira, E.M. Occurrence of Parabens in Surface Water, Wastewater Treatment Plant in Southeast of Brazil and Assessment of Their Environmental Risk. *Water, Air, Soil Pollut.* **2020**, *231*, 1–13.
- [29] Agunbiade, F.O.; Moodley, B. Occurrence and Distribution Pattern of Acidic Pharmaceuticals in Surface Water, Wastewater, and Sediment of the Msunduzi River, KwaZulu-Natal, South Africa. *Environ. Toxicol. Chem.* **2016**, *35*, 36–46.

- [30] Ebele, A.J.; Oluseyi, T.; Drage, D.S.; Harrad, S.; Abdallah, M.A.-E. Occurrence, Seasonal Variation and Human Exposure to Pharmaceuticals and Personal Care Products in Surface Water, Groundwater and Drinking Water in Lagos State, Nigeria. *Emerg. Contam.* **2020**, *6*, 124–132.
- [31] Ogunlaja, A.; Ogunlaja, O.O.; Olukanni, O.D.; Taylor, K.; Olorunnisola, C.G.; Dougnon, V.T.; Mousse, W.; Fatta-Kassinos, D.; Msagati, T.M.; Unuabonah, E.I. Antibiotic Resistomes and Their Chemical Residues in Aquatic Environments in Africa. *Environ. Pollut.* **2022**, *312*, 119783.
- [32] Adebawale, K.; Unuabonah, I.; Olu-Owolabi, B. Adsorption of Some Heavy Metal Ions on Sulfate-and Phosphate-Modified Kaolin. *Appl. Clay Sci.* **2005**, *29*, 145–148.
- [33] Tauc, J. *Amorphous and Liquid Semiconductors*; Springer Science & Business Media: New York, **2012**.
- [34] Mattar Knesebeck, A.; Ortiz, R.W.P.; Wypych, F.; Zanoelo, E.F. Synthesis of Malic Acid on Montmorillonite K10: A Langmuir-Hinshelwood Kinetic Study. *Ind. Eng. Chem. Res.* **2019**, *58*, 9257–9265.
- [35] Alfred, M.O.; Moodley, R.; Oladoja, N.A.; Omorogie, M.O.; Adeyemi, O.G.; Olorunnisola, D.; Msagati, T.A.M.; de Jesus Motheo, A.; Unuabonah, E.I. Sunlight-active Cu/Fe@ ZnWO<sub>4</sub>-Kaolinite Composites for Degradation of Acetaminophen, Ampicillin and Sulfamethoxazole in Water. *Ceram. Int.* **2021**, *47*, 19220–19233.
- [36] Severo, E.d.C.; Abaide, E.R.; Anchieta, C.G.; Foletto, V.S.; Weber, C.T.; Garlet, T.B.; Collazzo, G.C.; Mazutti, M.A.; Gündel, A.; Kuhn, R.C. Preparation of Zinc Tungstate (ZnWO<sub>4</sub>) Particles by Solvo-Hydrothermal Technique and Their Application as Support for Inulinase Immobilization. *Mater. Res.* **2016**, *19*, 781–785.
- [37] Cui, X.; Zhen Huang, W.; Zhou, H.; Yong Yin, H.; Fan Zheng, Y.; Chun Song, X. A Novel ZnS/ZnWO<sub>4</sub> Nanocomposite with Enhanced Photocatalytic Properties. *Curr. Nanosci.* **2015**, *11*, 360–365.
- [38] Cheng, Y.; Luo, F.; Jiang, Y.; Li, F.; Wei, C. The Effect of Calcination Temperature on the Structure and Activity of TiO<sub>2</sub>/SiO<sub>2</sub> Composite Catalysts Derived from Titanium Sulfate and fly ash Acid Sludge. *Colloids Surf. A: Physicochem. Eng. Asp.* **2018**, *554*, 81–85.
- [39] Unuabonah, E.I.; Günter, C.; Weber, J.; Lubahn, S.; Taubert, A. Hybrid Clay: A new Highly Efficient Adsorbent for Water Treatment. *ACS Sustain. Chem. Eng.* **2013**, *1*, 966–973.
- [40] Omorogie, M.O.; Agunbiade, F.O.; Alfred, M.O.; Olaniyi, O.T.; Adewumi, T.A.; Bayode, A.A.; Ofomaja, A.E.; Naidoo, E.B.; Okoli, C.P.; Adebayo, T.A.; Unuabonah, E.I. The Sequestral Capture of Fluoride, Nitrate and Phosphate by Metal-Doped and Surfactant-Modified Hybrid Clay Materials. *Chem. Pap.* **2018**, *72*, 409–417.
- [41] Olu-Owolabi, B.I.; Alabi, A.H.; Diagboya, P.N.; Unuabonah, E.I.; Düring, R. Adsorptive Removal of 2,4,6-Trichlorophenol in Aqueous Solution Using Calcined Kaolinite-Biomass Composites. *J. Environ. Manag.* **2017**, *192*, 94–99.
- [42] Meroufel, B.; Zenasni, M. Preparation, characterization, and heavy metal ion adsorption property of APTES-modified kaolin: comparative study with original clay, Springer 2018.
- [43] Lin, B.; Yan, Y.; Guo, M.; Cao, Y.; Yu, Y.; Zhang, T.; Huang, Y.; Wu, D. Modification-free Carbon Dots as Turn-on Fluorescence Probe for Detection of Organophosphorus Pesticides. *Food Chem.* **2018**, *245*, 1176–1182.
- [44] Feng, K.; Huang, S.; Lou, Z.; Zhu, N.; Yuan, H. Enhanced Photocatalytic Activities of the Heterostructured Upconversion Photocatalysts with Cotton Mediated on TiO<sub>2</sub>/ZnWO<sub>4</sub>:Yb<sup>3+</sup>,Tm<sup>3+</sup>. *Dalton Trans.* **2015**, *44*, 13681–13687.
- [45] Geetha, G.; Sivakumar, R.; Sanjeeviraja, C.; Ganesh, V. Photocatalytic Degradation of Methylene Blue dye Using ZnWO<sub>4</sub> Catalyst Prepared by a Simple co-Precipitation Technique. *J. Sol-Gel Sci. Technol.* **2021**, *97*, 572–580.
- [46] Mornani, E.; Mosayebian, P.; Dorrani, D.; Behzad, K. Effect of Calcination Temperature on the Size and Optical Properties of Synthesized zno Nanoparticles. *J. Ovonic Res.* **2016**, *12*, 75–80.
- [47] Gerischer, H. Photocatalysis in Aqueous Solution with Small TiO<sub>2</sub> Particles and the Dependence of the Quantum Yield on Particle Size and Light Intensity. *Electrochim. Acta* **1995**, *40*, 1277–1281.
- [48] Pereira, P.F.d.S.; Gouveia, A.; Assis, M.d.; De Oliveira, R.; Pinatti, I.; Penha, M.; Gonçalves, R.; Gracia, L.; Andrés, J.; Longo, E. ZnWO<sub>4</sub> Nanocrystals: Synthesis, Morphology, Photoluminescence and Photocatalytic Properties. *Phys. Chem. Chem. Phys.* **2018**, *20*, 1923–1937.
- [49] Zawawi, S.M.M.; Yahya, R.; Hassan, A.; Mahmud, H.E.; Daud, M.N. Structural and Optical Characterization of Metal Tungstates (MWO<sub>4</sub>; M= Ni, Ba, Bi) Synthesized by a Sucrose-Templated Method. *Chem. Cent. J.* **2013**, *7*, 1–10.
- [50] Kaczmarek, S.M.; Fuks, H.; Leniec, G.; Skibiński, T.; Jasik, A.; Tomaszewicz, E.; Groń, T. EPR Characterization of new Cadmium, Zinc and Rare-Earth Tungstates and Molybdates. *Curr. Top. Biophys* **2010**, *33*, 103–108.
- [51] Li, Y.; Tang, Z.; Zhang, J.; Zhang, Z. Defect Engineering of Air Treated-WO<sub>3</sub> and Its Enhanced Visible-Light-Driven Photocatalytic Performance and Electrochemical Performance. *J. Phys. Chem. C* **2016**, *18*, 9750–9763.
- [52] Bayode, A.A.; dos Santos, D.M.; Omorogie, M.O.; Olukanni, O.D.; Moodley, R.; Bodede, O.; Agunbiade, F.O.; Taubert, A.; de Camargo, A.S.; Eckert, H.; et al. Carbon-mediated Visible-Light Clay-Fe<sub>2</sub>O<sub>3</sub>-Graphene Oxide Catalytic Nanocomposites for the Removal of Steroid Estrogens from Water. *J. Water Process Eng.* **2021**, *40*, 101865.
- [53] Zhai, B.-g.; Yang, L.; Zhou, F.-f.; Shi, J.-s.; Huang, Y.M. Strong Photo-Oxidative Capability of ZnWO<sub>4</sub> Nanoplates with Highly Exposed {0 1 1} Facets. *Catalysts* **2019**, *9*, 178.
- [54] Wang, L.; Tsang, C.-S.; Liu, W.; Zhang, X.; Zhang, K.; Ha, E.; Kwok, W.-M.; Park, J.H.; Lee, L.Y.S.; Wong, K.-Y. Disordered Layers on WO<sub>3</sub> Nanoparticles Enable Photochemical Generation of Hydrogen from Water. *J. Mater. Chem. A* **2019**, *7*, 221–227.
- [55] Basyach, P.; Guha, A.K.; Borthakur, S.; Kalita, L.; Chetia, P.; Sonowal, K.; Saikia, L. Efficient Hydroxylation of Benzene to Phenol by H<sub>2</sub>O<sub>2</sub> Using Ni-Doped CuWO<sub>4</sub> on Carbon Nitride as a Catalyst Under Solar Irradiation and its Structure–Activity Correlation. *J. Mater. Chem. A* **2020**, *8*, 12774–12789.
- [56] Chen, C.; Bi, W.; Xia, Z.; Yuan, W.; Li, L. Hydrothermal Synthesis of the CuWO<sub>4</sub>/ZnO Composites with Enhanced Photocatalytic Performance. *ACS Omega* **2020**, *5*, 13185–13195.